ELSEVIER

Coordination Chemistry Reviews 143 (1995)
457–500

COORDINATION CHEMISTRY REVIEWS

# Pt–Re clusters and bimetallic catalysts

Jianliang Xiao, Richard J. Puddephatt*

*Department of Chemistry, The University of Western Ontario, London N6A 5B7, Canada*

Received 27 October 1994

**Contents**



**Abstract**

A review is given, from an organometallic perspective, of the current state of knowledge of the structure and activity of the bimetallic Pt–Re–$Al_2O_3$ catalysts used in petroleum reforming and of the known heteronuclear Pt–Re cluster complexes. Some comparisons between proposed structures, bonding and reactivity in the Pt–Re clusters present in the heterogeneous catalytic materials and in the well-defined clusters are made.

*Keywords:* Pt–Re clusters; Bimetallic catalysts; Petroleum refining

* Corresponding author.


*SSDI* 0010-8545(94)07008-3

## 1. Introduction

A large number of heteronuclear cluster complexes have been synthesized in the past two decades. The enormous interest in these clusters is stimulated mainly by the potential applications in catalysis, either as models or as precursors for bimetallic catalysts. Due to the wide use of platinum in catalysis, it is not surprising that much of this research has concentrated on clusters containing at least one platinum atom [1–3]. A recent comprehensive review summarised advances in recearch on heteronuclear clusters containing platinum and Group VIII transition metals [4]. This article focuses on clusters containing both platinum and rhenium with at least one metal–metal bond. There are still few such compounds compared with those containing platinum and group VIII metals. However, there is growing interest in complexes containing Pt–Re bonds, owing to the use of Pt–Re catalysts in naphtha reforming [5]. In this review, a brief account of the area of bimetallic Pt–Re catalysts is included, in hopes that the findings made by and the problems facing catalytic chemists may provide further impetus to the study of Pt–Re cluster complexes in particular, and of heteronuclear clusters in general. The account is mainly focused on studies reported in the last few years, and the interested reader is referred to previous reviews [5–10] and papers cited below. In addition, reviews on homonuclear rhenium cluster compounds are also available [11–13].

Bimetallic catalysts are widely used in industrial processes, and are playing a key role in the understanding of surface catalysis [5,10]. The introduction of a second metal to a monometallic catalyst can dramatically influence the catalytic properties, including factors such as stability and selectivity. The change may be due to electronic and/or geometric interactions between the metals. However, in most cases the complexity of these heterogeneous systems makes a complete understanding of the role of the second metal almost impossible. Therefore, modelling by using easily characterisable cluster complexes could provide important insight into the nature of interactions between the two metals in the catalysts.

## 2. Bimetallic Pt–Re catalysis

### 2.1. The formation and effectiveness of $Pt–Re/Al_2O_3$ catalysts

Among industrial bimetallic catalysts, oxide-supported Pt–Re catalysts have received the most attention, due to the use in naphtha reforming for the production of gasoline with high octane number. Other catalysts used in reforming include oxide-supported Pt, Pt–Sn and Pt–Ir systems [5–7,14]. The major reactions in reforming of saturated hydrocarbons include isomerization, dehydrogenation and dehydrocyclization to produce aromatic hydrocarbons, all of which improve the octane rating of gasolines. Another important type of reaction in reforming is hydrogenolysis of alkanes and cycloalkanes to give low molecular weight alkanes [14]. These reactions are illustrated in Scheme 1. Industrial catalysts have metals (about 1 wt %) dispersed on the surface of alumina, and the reforming reactions are

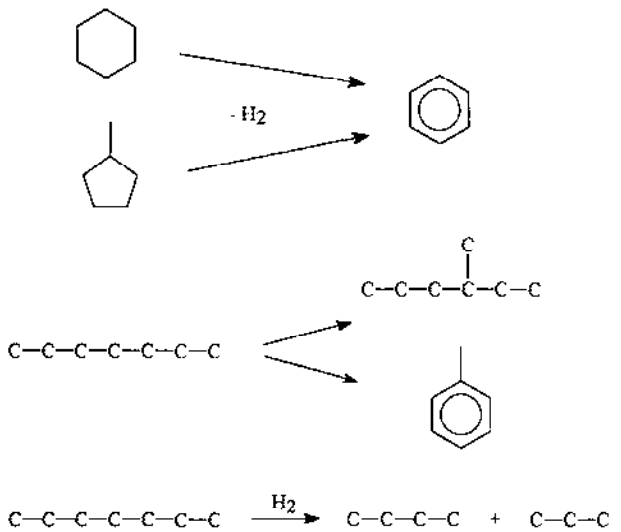


Scheme 1. Typical reactions in catalytic reforming.

carried out at temperatures of 700–800 K and pressures of 10–30 atm. However, the support is not an innocent partner, since the catalysts are in fact bifunctional, with metals catalyzing dehydrogenation and dehydrocyclization reactions, and the support, which is acidic, playing a role in catalyzing isomerization. Bimetallic Pt–Re catalysts are usually prepared by impregnation of alumina with aqueous solutions of compounds such as $H_2PtCl_6$ and $NH_4ReO_4$, followed by calcination in an oxygen atmosphere and then reduction under hydrogen. The catalysts are usually designated by Pt–Re/$Al_2O_3$ [14]. A new approach to bimetallic catalysts such as Pt–Re/$Al_2O_3$ is the use of mixed-metal cluster complexes as precursors [3]. An example is seen in the preparation of Pt–Re/$Al_2O_3$ from $[PtRe_2(CO)_{12}]$ [15]. A potential advantage of this new method is that the Pt–Re metal–metal bonds in the cluster might favour the preservation of bimetallic interactions in the final form of the catalysts.

The original reforming catalyst is based on alumina-supported platinum [14]. The addition of rhenium significantly improves the lifetime and selectivity for aromatics of the catalysts. As an example, the conversion of methylcyclopentane to benzene and C1–C6 alkanes over Pt/$Al_2O_3$ and Pt–Re/$Al_2O_3$ may be compared [16]. As can be seen from Table 1, after operating for 23.5 h, the activity, represented by conversion to all products, of the Pt catalyst drops by 23%, whereas that of the Pt–Re catalyst drops by only 2% compared to the initial activity. During the same period of time, the Pt/$Al_2O_3$ catalyst loses selectivity to benzene by 13%, while the Pt–Re/$Al_2O_3$ catalyst enjoys a gain of 5%. The results also shows that rhenium alone is not suitable as a catalyst for reforming reactions, since the major reactions it catalyzes are cracking to give alkanes [16]. The Pt–Re catalyst was introduced about two decades ago [17], and has been the subject of numerous investigations since that time [5–9,14]. The major questions that are still being debated are the

Table 1
Methylcyclopentane conversion over alumina-supported catalysts[a]

| Catalyst[b] | Time (h)[c] | % conversion[d] | % benzene | % alkanes |
|---|---|---|---|---|
| Pt(0.3) | 0.5 | 40 | 79 | 21 |
| | 24 | 17 | 66 | 34 |
| Re(0.3) | 0.5 | 17 | 16 | 84 |
| | 24 | 13 | 25 | 75 |
| Pt(0.3)Re(0.3) | 0.5 | 38 | 71 | 29 |
| | 24 | 36 | 76 | 24 |

[a] Ref. [16].
[b] Number in parenthesis is metal loading in wt%.
[c] On stream time for the catalysts.
[d] Obtained with methylcyclopentane containing 1 ppm sulfur at 773 K, 14.6 atm, and $H_2$/methylcyclopentane (mol $mol^{-1}$) = 5.

nature of the interaction between the two metals, the role of rhenium in maintaining catalytic activity and the oxidation state of rhenium. For clarity, the oxidation state of Re is discussed first.

Before addressing the details, it may be helpful to explain some terms that frequently appear in catalytic journals but which may not be familiar to organometallic chemists. Two frequently used terms are the electronic effect and the ensemble or geometric effect, with the former referring to the change in the electronic structure of element A upon the addition of B, and the latter describing changes in the active site distribution of A upon the addition of B. They are thus related to the terms electronic effect and steric effect in coordination chemistry. The term bimetallic clusters used in catalysis refers to metallic entities which are highly dispersed on the surfaces of the support, but in which it is usually not known if metal–metal bonds are present. Another frequently used term is alloy, which refers to the same mixed metal particles, and is not necessarily identical to a bulk alloy, although it assumes the presence of metal–metal bonding. In order to avoid confusion with molecular clusters, the term alloy is used throughout this article.

### 2.2. *The oxidation state of Re*

As mentioned, Pt–Re/$Al_2O_3$ catalysts are normally reduced prior to use. The oxidation state of Pt in the reduced catalysts is widely accepted to be zero. However, the oxidation state of Re in the reduced catalysts has been debated for a long time and the issue is still unresolved [5,6,8,9,14,18–33]. For the Pt–Re/$Al_2O_3$ catalysts, where formation of alloys is suggested (see Section 2.3), it is believed that both Pt and Re are in the metallic state [20,24–30]. Evidence for this arises mainly from investigations of temperature-programmed reduction (TPR) [24–26,29], X-ray photoelectron spectroscopy (XPS) [27,28] and X-ray absorption spectroscopy (XAS) [20,22,30] of the catalysts. An example is seen in the X-ray absorption edge studies of a Pt–Re/$Al_2O_3$ catalyst that is reduced at about 773 K in $H_2$, showing that the

$L_{III}$ edge intensity of the Re closely matches that of bulk Re instead of $ReO_4^-$, indicating that rhenium is present as Re(0) in the catalyst [8,20]. In conjunction with TPR, a similar XAS study, where binding energy instead of edge intensity is used to determine the degree of Re reduction, concludes that Re in Pt-Re/$Al_2O_3$ is completely reducible to Re(0) if a sufficiently high reduction temperature is used for samples previously calcined at low temperature. The study also suggests that the use of $L_{III}$ edge intensity is inadequate to characterize the oxidation state of the metals in Pt–Re/$Al_2O_3$ [22]. In a different approach, Re is alloyed with a Pt metal film, and is then oxidized by heating the alloy in oxygen, followed by reduction at 573 K in hydrogen. The photoelectron spectrum of the reduced alloy displays the Re $4f_{7/2}$ peak at 39.7 eV binding energy, the same as observed for Re metal (Table 2) [28].

However, the presence of cationic rhenium, in particular Re(IV) and Re(II), has also been suggested by virtue of the same physical techniques [15,19,21,31]. An early example is found in the application of both XPS and XAS in following the reduction of commercial type Pt–Re/$Al_2O_3$ catalysts at 733–758 K in $H_2$, showing that metallic Pt and Re(IV) (the Re $4f_{7/2}$ binding energy is found to be about 42.2 eV, see Table 2 for comparison) are the dominant species after reduction [33a]. However, caution should be taken since the conclusion in this study is partly derived from the comparison of the $L_{III}$ edge intensities of various Re species. An ESR study also confirms the existence of Re(IV) along with Re(0) in Pt–Re/$Al_2O_3$ reduced at 773 K, but the former accounts for less than 10% of the Re in the catalyst [31]. A recent study of Pt–Re/$Al_2O_3$, using TEM/EDX analysis on a catalyst reduced at 673 K, shows that the majority of rhenium is present as $ReO_2$ [33b].

Some recent EXAFS studies also tend to indicate a cationic form for Re [19,21]. Thus, in two separate studies, analysis of EXAFS data on Pt–Re catalysts shows that Re has an oxygen coordination number of 1.4 and 3.2, respectively, with Re–O distances ranging from 2.10 to 2.57 Å. The catalysts are supported on alumina [21] and zeolite [19], and reduced at 733 K and 558 K in $H_2$, respectively. For comparison, it is noted that the metal–oxygen single bond distances in a number of complexes falls in the range 2.1 to 2.2 Å [34]. An example is $[Re_2(CO)_6(\mu\text{-}OPh)_3]^-$ in which the Re–O distance is 2.14 Å [35]. Re has been found to interact strongly with oxide surfaces [15, 36–38]. For instance, decomposition of $[PtRe_2(CO)_{12}]$ on $Al_2O_3$ in

Table 2
XPS binding energies (eV) for Re samples[a]

| Sample | Re $4f_{7/2}$ |
|---|---|
| Re(metal) | 39.7 |
| $[Re(CO)_3(OH)]_4$ | 40.2[b] |
| $ReO_2$ | 42.5 |
| $ReO_3$ | 44.9 |
| $Re_2O_7$ | 46.7 |

[a] Ref. [28]. [b] Ref. [15].

hydrogen at 423 K yields a Re carbonyl species with $\nu(CO) = 2032$, 1925 and 1903 $cm^{-1}$. The species is formulated as $[Re(CO)_3\{O-Al\}\{HO-Al\}_2]$, where the braces refer to groups connecting to the bulk alumina [15]. Similar results are obtained by decomposing $[HRe(CO)_5]$ and $[H_3Re_3(CO)_{12}]$ on MgO, for which an EXAFS study shows that the $Re(CO)_3$ species is bound to three oxygen atoms from the support at distances of 2.13–2.15 Å [34,36]. Taken together, these studies indicate that, in the Pt–Re catalysts mentioned, much of the Re exists in a positive oxidation state and interacts strongly with the surface oxygens. However, the presence of the cationic Re species in the catalysts could be a result of the reduction temperature that may not be high enough. This is illustrated in the reduction of alumina-supported $[PtRe_2(CO)_{12}]$ at different temperatures in $H_2$. When the catalyst is reduced at 523 K, the Re $4f_{7/2}$ binding energy is found to be 41.3 eV, indicating that Re is present as Re(II). However, at 673 K, the binding energy decreases to 40.5 eV, corresponding to either Re(I) or Re(0) [15].

The above studies show that the pretreatment undergone by the catalyst has a profound effect on its reduction profile. In general, the higher the calcination (oxidation) temperature the more difficult is the subsequent reduction of the Re [22,25,26,29]. In addition, Pt has been found to catalyze the reduction of Re, and this effect appears to be observable only for catalysts calcinated at low temperature. As an example, reduction of Re, supported on alumina and pretreated in $O_2$ at 373 K, takes place at about 900 K. In contrast, co-reduction of both Pt and Re in $Pt–Re/Al_2O_3$ occurs at less than 573 K under similar conditions. On the other hand, when the bimetallic catalyst is pretreated in $O_2$ at 773 K, the reduction of Re is little affected by the presence of Pt [29]. Detailed studies have indicated that this catalytic effect of Pt on the reduction of Re is most effective only when Pt and Re are in close proximity. An XPS study on Pt and Re films shows that when Re is layered on and so not intimately mixed with Pt, its reduction is not complete, with a mixture of Re(0) and ReO being formed, but when the two metals are alloyed, Re is completely reduced to Re(0). In both cases, Pt is reduced to the metallic state [28]. Another illustrative example is seen in the comparison of the reduction of catalysts prepared from $[PtRe_2(CO)_{12}]$ and by physically mixing $Re/Al_2O_3$ with $Pt/Al_2O_3$. When reduced at 673 K in $H_2$, the Re in the former is reduced to either Re(I) or Re(0), whereas in the latter it is present as Re(VII) (the Re $4f_{7/2}$ binding energy is observed at 47.7 eV) [15]. A mechanism accounting for the catalytic phenomenon is that hydrogen is activated by zero-valent Pt centres, so when Pt and Re are in close proximity, the reduction of the Re may be facilitated by "hydrogen spillover" [25,28,29]. But it is noted that, even in the absence of hydrogen, Pt is also found to be able to catalyze the reduction of Re oxides [27]. In the case where Pt and Re are separated, migration of rhenium oxides towards metallic Pt is possible. However, when the catalyst is pretreated at high temperature, this migration may be inhibited by strong interactions between the rhenium oxides and the support surfaces, thus making the reduction of Re more difficult [25]. Several studies have shown that the oxidic Re species is $ReO_4^-$ on hydrated $Al_2O_3$ surfaces at low temperature, but that Re–O–Al bonds are formed at elevated temperature, as illustrated in Scheme 2 [37,38].

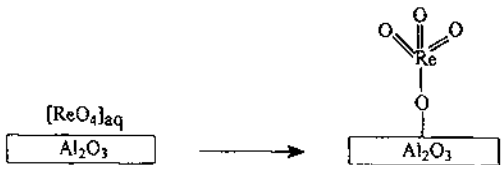


Scheme 2.

### 2.3. The nature of the interaction between Pt and Re

With regard to the nature of interaction of the two metals, the very first question we have to address is whether there is significant bimetallic interaction in the reduced catalyst. The results from various studies are controversial, but the balance of the evidence is in favour of the presence of Pt–Re interactions [15,18–21,25–33,39–41]. An earlier study, which contradicts the idea of bimetallic interactions, was made on a physical mixture of $Pt/Al_2O_3$ and $Re/Al_2O_3$, which displays about the same stability as a $Pt–Re/Al_2O_3$ catalyst. Cross contamination between Pt and Re is not detected in the physical mixtures. It is therefore suggested that Pt and Re are present as segregated surface entities and there exist no Pt–Re interactions [41]. On the other hand, it has been found that Re oxides can migrate over the surface of alumina with which it is physically mixed [29, 42]. Further, trace amounts of Re, which may not be easy to detect by physical means, could have a significant effect on catalytic reactions such as hydrogenolysis [43]. Therefore, the existence of Pt–Re interactions in physical a mixture of Pt and Re catalysts may not be completely excluded. A recent study using TEM/EDX techniques, indicated that platinum is present in metallic form, rhenium is present as $ReO_2$ and that there is no significant alloy formation. The role of Re is then to modify the alumina support surface [33b].

The most significant results in support of bimetallic interactions stem from extended X-ray absorption fine structure (EXAFS) investigations. Table 3 shows the results obtained from a reduced Pt (1 wt %)Re(1 wt %)/$Al_2O_3$ catalyst [30,44]. As can be seen, significant coordination of Re to Pt takes place, and the Pt–Re distance is unusually short, at 2.64 Å. In molecular Pt–Re complexes where a clear Pt–Re bond has been identified, the Pt–Re distances are often found in the range 2.71 to 2.90 Å (see below). In fact, the Pt–Re distance of 2.64 Å is shorter than the Pt–Pt or

Table 3
Coordination in $Pt–Re/Al_2O_3$ catalysts[a]

| Bond | Distance (Å) | Coordination number[b] |
|---|---|---|
| Pt–Pt | 2.75 | 4.8 |
| Pt–Re | 2.64 | 2.9 |
| Re–Pt | 2.64 | 2.9 |
| Re–Re | 2.73 | 4.2 |

[a] Refs. [30,44]. These data are for a 1:1 Pt:Re catalyst.
[b] Number of second metal atoms around first metal atom.

Re–Re distances found in the pure metals (2.775 Å for Pt and 2.750 Å for Re) [30], indicating the formation of an alloy containing strong Pt–Re bonds. EXAFS data also reveal that the alloy particles formed on the surfaces of the support are not uniform, having regions rich in Pt and other regions rich in Re. It is also interesting to note that the incorporation of sulfur does not disrupt the bimetallic clusters, as indicated by the Pt–Re distance of 2.65 Å in the sulfided catalyst in comparison with that of 2.64 Å in the unsulfided catalyst. A synchrotron anomalous X-ray diffraction study shows that the structure of most Re in Pt–Re/$SiO_2$ is different from that in bulk Re but closely matches that of Pt, an indication of a strong bimetallic interaction in the catalyst [45]. In these and other alloy-type Pt–Re catalysts, both Pt and Re are believed to be in the metallic state.

As pointed out in Section 2.2, Re may also exist as cationic species and may interact strongly with the support. Evidence has been put forward to show that such Re cations also interact with Pt by inhibiting the agglomeration of the latter. For example, in the zeolite-supported Pt–Re catalyst, reduction at 558 K in $H_2$ give a Pt–Pt coordination number 8.2 in the absence of Re, which corresponds on average to Pt clusters 12.5 Å in diameter, but 5.1 when Re is present, corresponding to Pt clusters 6.7 Å in diameter. In addition, when the reduction temperature is raised from 458 to 558 K, the increase in the size of the Pt clusters in the absence of Re is found to be an order of magnitude larger than that in the presence of Re. It is therefore concluded that Re markedly inhibites the agglomeration of Pt, supporting the existence of Pt–Re interactions [19]. In the catalysts studied, Re is cationic and bound to surface oxygen atoms of the support, and so is not alloyed with Pt. A sandwich model has been proposed to explain the structure of analogous Pt–Re catalysts, in which the cationic Re species is sandwiched between Pt and the support, and acts as an anchor to inhibit Pt agglomeration so that a high dispersion of Pt is maintained [46,47]. On the other hand, an in situ EXAFS study has shown that under conditions close to practical reforming, that is, in the presence of both $H_2$ and hydrocarbon at high temperature, the coordination of oxygen to Re is decreased [21]. Therefore it is possible that in practical reforming the metals in the sandwich structure could become alloyed, with both Pt and Re in the metallic state. A similar sandwich model has been proposed for zeolite-supported Pt–Cr systems, in which the outermost layer consists of Pt and the second shell is enriched with Cr [48,49].

Another important method for characterizing alloy formation is by study of chemical reactions, particularly catalytic hydrogenolysis and the adsorption and desorption of small molecules. For hydrocarbon hydrogenolysis, where carbon–carbon bond cleavage is involved, several contiguous surface atoms are required, that is, the ensemble requirement is large. Both Pt and Re are known to catalyze hydrogenolysis reactions, with the latter being the more reactive [7]. However, studies have shown that, when Re is added to Pt, the resultant catalysts behave differently, being more reactive in hydrogenolysis than either the monometallic catalysts or their physical mixture [24,32,43,50]. A good example is found in the results of a study on ethane hydrogenolysis over unsupported bimetallic crystal surfaces. Thus, although the Re(0001) surface is found to be two orders of magnitude more reactive than the Pt(111) surface, a bimetallic surface of composition $Re_2Pt$

displays an activity about one order of magnitude higher than the Re(0001) surface, indicating that the activity of the bimetallic surface does not correspond to a linear combination of the monometallic surfaces [43]. Similar results have also been obtained for supported Pt–Re catalysts [24,32,50]. For instance, in hydrogenolysis of cyclopentane, the turnover frequency for methane formation over the catalyst that is prepared by co-impregnation and co-reduction exceeds that of a physical mixture by a factor of 40, matching the results observed for macroscopic, unsupported Pt–Re alloys [32,51]. In line with these observations, chemisorption of $H_2$ and CO on bimetallic Pt–Re surfaces is shown to be different than on either Pt or Re surfaces, with the maximum adsorption of $H_2$ and CO occurring on the bimetallic surfaces containing 0.15 to 0.3 monolayer of Re on Pt(111) [52]. Taken together, these results indicate that a Pt–Re alloy is formed, in which Re interacts with Pt.

The nature of the Pt–Re interactions has been explained mainly in terms of electronic and ensemble effects. For the majority of supported Pt–Re catalysts, in which formation of Pt–Re alloy is claimed, the ensemble effect has been suggested as the main cause of their superior selectivity and stability [24–26,29,31,32,50]. Alloying Re with Pt will certainly change to some extent the ensembles of Pt active sites, giving rise to the formation of mixed Pt–Re ensembles. Pt–C bonds are possibly weaker than Re–C bonds, so the rate-determining step in hydrogenolysis on Pt could be the fission of C–C bonds, but that on Re could be the desorption of the products such as methane. Thus the high activity for hydrogenolysis displayed by Pt–Re alloy catalysts may be explained by assuming that the mixed ensemble has a more appropriate metal–carbon bond strength than either pure Re or Pt. If this is the case, varying the composition of the Pt–Re catalyst should allow a maximum to be observed in the activity for the hydrogenolysis. This has indeed been observed in the hydrogenolysis of cyclopentane, where the highest activity is observed for a catalyst with about 34% Pt and 66% Re [53], reminiscent of the result obtained from the bimetallic surface discussed above [43]. Hydrogenolysis produces small alkane molecules and the reaction is highly exothermic, so the the industrial alloy catalyst has to be sulfided in order to suppress this reaction [7]. In both the unsulfided and the sulfided catalysts, there may exist electronic interaction between Pt and Re. For example, shifts are observed in both $\nu$(CO) stretching frequencies for CO adsorbed on Pt and Pt $4f_{7/2}$ binding energy on going from $Pt/SiO_2$ to $Pt–Re/SiO_2$, as shown in Table 4 [51]. However, it has been argued, by analyzing $^{12}CO$ and $^{13}CO$ adsorption, that evidence such as this do not support the existence of significant electronic interactions, and that the effect of this interaction is minor [54]. In the sandwich model, geometric interaction between the two metals is realized by the Re anchor that inhibits agglomeration of Pt, but electronic modification of Pt by the Re cations is also suggested [46–49].

Although direct spectroscopic evidence for an electronic effect is ambiguous in the supported Pt–Re catalysts, the importance of this effect has been indicated in various studies of bimetallic surfaces [27,28,43,52]. As mentioned, Pt(111) is less reactive than Re(0001) in ethane hydrogenolysis. However, when the Re(0001) surface is partly covered by Pt, the resultant surface displays a higher instead of a lower activity in hydrogenolysis. Further study shows that this is not due to the ensemble

Table 4
IR data and XPS binding energies (eV) for silica-supported catalysts[a]

| Sample | $\nu$(CO) ($cm^{-1}$) | Pt $4f_{7/2}$ | Re $4f_{7/2}$ |
|---|---|---|---|
| Pt | 2050 | 71.6 | |
| Re | | | 40.5 |
| PtRe | 2090 | 72.0 | 40.7 |
| PtRe(S) | 2070 | 72.1 | 40.8[b] |

[a] Ref. [51].
[b] Sulfided catalyst; about 20% of the peak was shifted to higher energy and the value given is for the lower energy Re(0) component [51].

effect proposed for the alloy catalysts. Thus when the Re surface is fully covered by a monolayer of Pt, the activity of the surface is found to be quite close to that of the clean Re(0001) [43]. These results are difficult to explain solely in terms of the ensemble effect, but are consistent with the electronic structure of Pt being modified by Re. In addition, it is noted that following deposition of Re on Pt(111), the Pt $4f_{7/2}$ binding energy increases from 70.9 eV to 71.4 eV [27]. Although the cause of this shift is not clearly defined, studies carried out on other bimetallic surfaces have shown quite clearly that a large change in the electron density of a metal can be induced by alloying [10]. For example, when Pd is supported on metals such as Ta(110), W(110) and Re(0001), transfer of electron density occurs from Pd to the substrate [55]. This change in electronic state is likely to cause perturbation in the chemical properties of the components of the bimetallic system. Indeed, it has been found that a decrease in CO binding energy, which can be measured by the decrease in CO desorption temperature from the the monolayer, is accompanied by an increase in the binding energy of the Pd atoms in the monolayer. As an example, for the Ru(0001) supported Pd monolayer, the increase in the Pd $3d_{5/2}$ binding energy is observed to be 0.30 eV relative to pure Pd(100), and CO desorbs from the monolayer at temperature 120 K lower than that found from pure Pd(100). In comparison, for Pd/Ta(110) the increase in Pd $3d_{5/2}$ binding energy is 0.90 eV, corresponding to a decrease of 235 K in CO desorption temperature [55]. For the Pt–Re surfaces, analogous observations regarding $H_2$, but not CO, desorption have been made [52]. As shown in Table 5, although the $H_2$ desorption temperature from clean Re(0001) is 50 K higher than from Pt(111), deposition of Re on Pt(111) causes a continuous decrease in the $H_2$ desorption temperature. Another interesting observation is that maximum $H_2$ adsorption is obtained from the surface with $\theta_{Re}=0.19$, that is, 0.19 monolayer of Re, and this surface holds 20% more $H_2$ than pure Pt(111) does [52]. The increase in hydrogen surface concentration has also been observed for supported Pt–Re systems [18,56]. Therefore, for supported catalysts the electronic effect could be equally important as the ensemble effect.

In the sulfided catalysts, the Pt–Re alloy particles probably remain intact, as indicated by the EXAFS study [30]. Sulfur is more strongly bound to Re than to Pt in the bulk [57]. This also appears to be true at surfaces, as indicated by the

Table 5
Hydrogen desorption temperatures obtained from Re modified Pt(111)[a]

| $\theta_{Re}$[b] | T (K) |
|---|---|
| 0 | 410 |
| 0.19 | 398 |
| 0.66 | 370 |
| 1.3 | 336 |
| ∞ | 460[c] |

[a] Ref. [52]. [b] Re coverage. [c] Pure Re(0001) surface.

observation that supported Pt–Re systems retain more sulfur than supported Pt [58,59]. Therefore it is generally believed that in the bimetallic Pt–Re alloys sulfur is selectively chemisorbed on Re. However, direct evidence regarding the whereabouts of sulfur appears sparse. The XPS data given in Table 4 shows that part of the Re $4f_{7/2}$ signal for Pt–Re/$SiO_2$ is shifted to higher energy than that found for the unsulfided Pt–Re/$SiO_2$. In contrast, no significant change is detected for Pt. The result is consistent with surface Re being sulfided [51]. Reforming of *n*-heptane over Pt–Re/$Al_2O_3$ shows that sulfur coverage (mole S/mole metal exposed) of 0.28 is sufficient to suppress hydrogenolysis, and further addition of sulfur leads to detrimental changes in selectivity towards isomerization and dehydrocyclization [58]. In the sulfided catalysts, the change in selectivity is suggested to be mainly steric in origin, with larger Pt ensembles being segregated to smaller ones by the Re–S units. A schematic illustration of Pt/$Al_2O_3$, Pt–Re/$Al_2O_3$ and sulfided Pt–Re/$Al_2O_3$ catalysts is given in Scheme 3, assuming that sulfur adsorbs on Re.

### 2.4. The role of Re in maintaining activity

Perhaps the most significant effect of adding Re to a monometallic Pt catalyst is increased stability. Deactivation of reforming catalysts is mainly caused by coke deposition on the catalyst surface, which involves successive fragmentation and dehydrogenation of hydrocarbons and reorganization of the resultant carbon species to graphitic carbon overlayers. Such reactions are favoured on large ensembles,

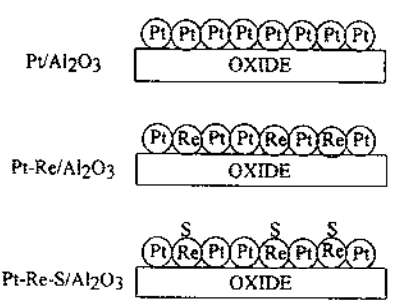


Scheme 3. Schematic illustration of oxide-supported Pt-Re catalysts.

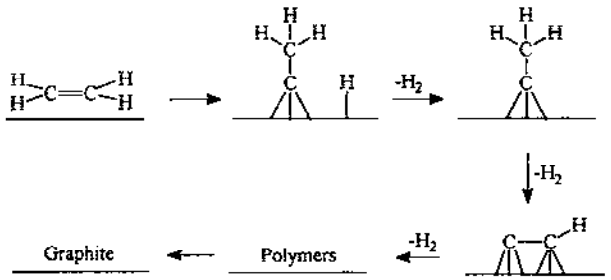


Scheme 4. Fragmentation of ethylene on Rh(111) with increasing temperature.

where multiple bonds can be easily formed between metal and hydrocarbons [7]. The coking process may be illustrated by the fragmentation of ethylene over Rh(111), which leads to polymeric species and eventually to graphitic structures with increasing temperature, as shown in Scheme 4 [60]. A model study indicates that most of the surfaces of working Pt reforming catalysts are continuously covered by a polymeric residue, which can easily exchange hydrogen with reacting molecules. However, with increasing time and temperature, this residue completely dehydrogenates, and condenses to graphitic species, leading to the deactivation of the catalysts [60]. It is now accepted that there are two distinct types of carbonaceous deposits, namely, reversible coke and irreversible coke. The former has an atomic H/C ratio of 1.5–2.0 and is readily removed by hydrogenation, and the latter has a H/C ratio of about 0.2 and is not revolatilized under reforming conditions [7].

According to the ensemble effect, the superior stability of the Pt–Re catalyst is due to the presence of inactive Re–S units that subdivide large Pt ensembles into smaller ones, so the transformation of reversible coke to graphitic entities, the irreversible coke, is inhibited. That is, although coke is deposited on both the Pt–Re and the Pt catalysts, it is less toxic to the former. Further, the formation of the irreversible coke may also be hindered sterically by the strongly chemisorbed sulfur [7,61]. This change in the nature of the deposited coke with the addition of Re and S is clearly evidenced by the results shown in Table 6. As can be seen, carbon deposition decreases from 354 to 99.0 $\mu$mol (g-cat)$^{-1}$ on going from $Pt/Al_2O_3$ to $Pt–Re(S)/Al_2O_3$, and the carbon species is much richer in hydrogen over the sulfided Pt–Re than over the Pt catalyst, with H/C = 1.84 for the former and 0.36 for the latter [61].

Table 6
Carbon and hydrogen retained on alumina-supported catalysts[a]

| Catalyst | C[b] | H[b] | H/C |
|---|---|---|---|
| Pt | 354 | 128 | 0.36 |
| PtRe | 216 | 51.4 | 0.24 |
| PtRe(S) | 99.0 | 182 | 1.84 |

[a] Ref. 61. [b] $\mu$mol (g-catalyst)$^{-1}$.

The ensemble effect accepts that it is the combined effect of both Re and S that gives rise to the observed stability for the Pt–Re catalysts [7,50,61]. In the absence of sulfur, the mixed Pt–Re ensembles in the alloy catalysts are highly reactive in hydrogenolysis as discussed earlier, and may deactivate quickly since C–C bonds fission and reorganisation can lead to graphitic species [7]. For instance, for the $Pt/Al_2O_3$ and the $Pt–Re/Al_2O_3$ catalysts in Table 6, the steady-state activity of the former is decreased from the initial by 43% while that of the latter by 57%. Surprisingly, the carbon deposition is less over the bimetallic catalyst, an observation also supported by other studies by using pure hydrocarbons [56,62,63]. However, the H/C ratios observed for the two catalysts are close, and much lower than that for $Pt–Re(S)/Al_2O_3$ (Table 6). The same study also indicated that the high H/C ratio observed for the $Pt–Re(S)/Al_2O_3$ is not only due to the presence of sulfur but also to the existence of Pt–Re interactions [61].

On the other hand, Re alone has been suggested to be able to change the nature of coke deposition [21,63]. For example, an EXAFS study of catalysts used for *n*-pentane reforming at 733 K reveals a Pt–C bond of 1.94 Å long for a $Pt/Al_2O_3$ catalyst, but no metal–carbon bonds for a $Pt–Re/Al_2O_3$ catalyst. The result may be explained in terms of the carbonaceous deposit being more highly hydrogenated and so less organized on the bimetallic catalyst than on the $Pt/Al_2O_3$, and so consequently the metal–carbon bond is not detected by EXAFS. In the catalyst studied, Re is found to force Pt to be more dispersed on the support surface, and formation of a Pt–Re intermetallic phase is suggested, which inhibits the graphitization of less harmful coke [21]. Highly dispersed Pt entities are more resistant to coke deposition [7], a result possibly due to the ensemble effect. Relevant to this is the sandwich model, where a high dispersion of Pt is maintained by cationic Re anchors bound to surface oxygen atoms. As mentioned, this model also assumes that Re modifies the electronic properties of Pt [46–49]. The supported Pt–Cr catalysts, used as models for the reforming catalysts, are suggested to have a sandwich structure, in which a Pt–Cr electronic interaction is assumed to reduce the metal–carbon bond strength. Together with the ensemble effect, this electronic interaction is responsible for the effect of Cr on the catalytic properties of Pt [48,49]. In addition, Re is known to increase surface hydrogen concentration on Pt–Re catalysts. Since graphitization involves deep dehydrogenation, a high hydrogen concentration, which is beneficial to the removal of coke by hydrogenation, should inhibit this process [18,52,56]. However, there are other studies, which indicate that Re alone could destroy coking precursors without alloying with Pt [39,41].

### 2.5. *Summary and relevance of model clusters*

In summary, recent results tend to indicate that, in supported Pt–Re catalysts, Re is largely reduced to the zero oxidation state, and alloys with Pt. However, there remains a possibility that some rhenium is in a higher oxidation state, and Re–O bonding may occur with the support material. The ensemble effect appears to be generally accepted as important in influencing catalytic activity and selectivity, particularly in the presence of sulfur. However, because of the difficulties of character-

izing heterogeneous catalysts, our understanding of the structure of the catalysts and of the role of Re in maintaining catalyst stability is incomplete. It is in this context that model clusters may contribute to a fuller understanding. Some questions that may particularly be of interest to organometallic chemists are: (1) In Pt–Re alloy particles is there any effect of Re on the electronic and chemical properties of Pt and vice versa, and can this lead to cooperative effects in terms of reactivity? (2) Is it true that sulfur preferentially binds to Re in Pt–Re alloys and, if so, how does the Re–S fragment affect the electronic structure and chemical reactivity of the platinum? (3) How does platinum catalyze the reduction of rhenium in the formation of Pt–Re catalysts? How does the oxidation state of Re affect the chemical behaviour of Pt–Re clusters and is it possible that Re–O bonding occurs at the Pt–Re/support interface?

In the following sections, the chemistry and structure of molecular Pt–Re clusters are described. The review will also include binuclear complexes having Pt–Re bonds. For simplicity, the discussion starts with these binuclear Pt–Re complexes, followed by clusters of higher nuclearity.

## 3. Binuclear Pt–Re complexes

There are several synthetic routes for Pt–Re cluster complexes, and the most frequently used method involves the use of Pt(0) compounds, which are highly reactive and can readily form metal–metal bonds by reaction with Re–X or Re=X bonds, usually with loss of one or more coordinated ligands. Detailed examples are found in this section and Section 4. For discussions of systematic synthesis of mixed-metal clusters, earlier reviews should be consulted [2,4,64,65].

### *3.1. Synthesis using alkylidene complexes*

The earliest binuclear Pt–Re bonded complex was prepared by the reaction of a Pt(0) complex with a mononuclear alkylidene complex. Thus mixing $[Pt(C_2H_4)L_2]$ (L = $PMe_3$ or $PMe_2Ph$) and $[CpRe\{C(OMe)C_6H_4Me\text{-}4\}(CO)_2]$ at room temperature yields the alkylidene-bridged complex **1**, as shown in Scheme 5 [66]. Treatment of **1** with $[OMe_3][BF_4]$ removes the OMe substituent at the alkylidene carbon, resulting in the formation of the alkylidyne-bridged complex **2**. The carbon atom of the alkylidyne ligand is susceptible to nucleophilic attack. Thus when **2** is treated with [NaOMe], **1** is regenerated, and with phosphines, the cationic species **3** is produced

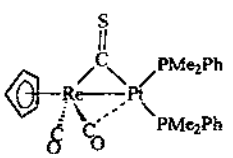


4

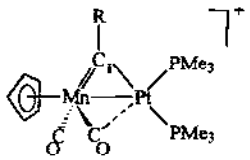


5 (R = $C_6H_4Me$-4)

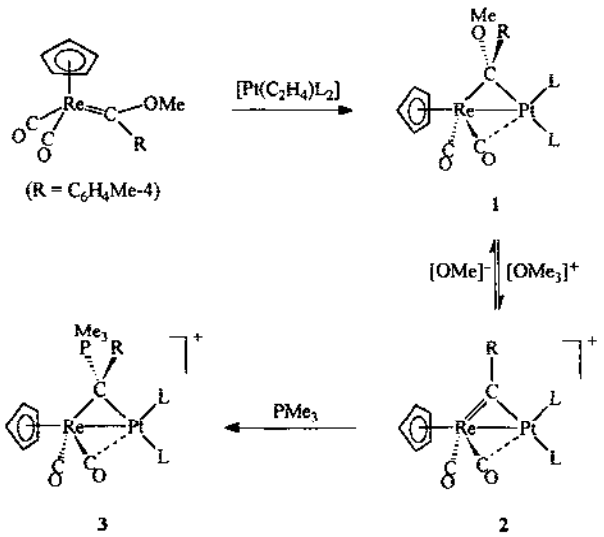


Scheme 5. (a, L = $PMe_3$; b. L = $PMe_2Ph$).

[67]. By the same method, the CS-bridged Pt–Re complex, **4**, is synthesized [68]. These complexes are characterized spectroscopically. Their $^{13}C$ NMR spectra are interesting. For the neutral alkylidene species, the bridging carbon appears at $\delta$ 166.0 for **1a** and 165.4 for **1b**. In comparison with the value of $\delta$ 288.1 observed for the mononuclear alkylidene complex $[CpRe\{C(OMe)C_6H_4Me\text{-}4\}(CO)_2]$, the alkylidene carbons in **1** are more shielded. For the cationic alkylidyne complexes, the bridging carbons are observed at $\delta$ 385.2 for **2a** and 382.6 for **2b**. Interestingly, these carbons are more deshielded than the alkylidyne carbon in $[CpRe(CC_6H_4Me\text{-}4)(CO)_2]^+$ ($\delta$ 315.3) [66].

The formation of the alkylidene complexes appears to be frontier orbital controlled, involving the interaction of the filled $b_2$ orbital of a $PtL_2$ fragment generated from $[Pt(C_2H_4)L_2]$ with the LUMO of the mononuclear alkylidene complex. Since mononuclear alkylidene complexes, which contain metal–carbon double bonds, are related to ethylene, and a $PtL_2$ fragment is isolobal to $CH_2$, the formation of these metallocyclopropane complexes from the two fragments thus follows logically. Likewise, the alkylidyne complex can be related to a cyclopropene molecule [65,68].

Using the same strategy, a variety of heteronuclear complexes analogous to **1** and **2** have been prepared [65,69]. Structure determination reveals that the alkylidene and alkylidyne carbons do not symmetrically bridge the metal–metal bond. For instance, in complex **5**, the Mn–C1 bond distance [1.829(8) Å] is shorter than the Pt–C1 bond distance [1.967(8) Å]. The former is also substantially shorter than Mn–C $\sigma$ bonds, but comparable with the Mn–C (alkylidene) bond in $[CpMn\{C(COPh)Ph\}(CO)_2]$ (1.88 Å), suggesting that the Mn–C1 linkage is a double bond. X-ray diffraction also reveals that one of the carbonyl ligands is semi-bridging, with the angle Mn–C–O = 157.5(9)° [66].

Table 7
Structurally characterized Pt–Re clusters

| Entry | Cluster | Geometry | Pt–Re[a] | Re–Re[a] | Ref. |
|---|---|---|---|---|---|
| **6** | $[PtRe(Cp)H_2(CO)_2(PPh_3)_2]$ | Binuclear | 2.838(1) | | 70a |
| — | $[PtRe(\mu\text{-}CH_2)(Cp)(CO)_2(PPh_3)_2]$ | Binuclear | 2.730(1) | | 72b |
| **10b** | $[PtRe(\mu\text{-}PCy_2)(Cp)H(NO)(PPh_3)_2]^+$ | Binuclear | 2.8675(5)[b] | | 74 |
| **11a** | $[PtRe(\mu\text{-}H)(\mu\text{-}PPh_2)(Cp)(NO)(PPh_3)_2]^-$ | Binuclear | 2.8673(4)[b,c] | | 74 |
| **11b** | $[PtRe(\mu\text{-}H)(\mu\text{-}PCy_2)(Cp)(NO)(PPh_3)_2]^+$ | Binuclear | 2.8815(8)[b,c] | | 74 |
| **14** | $[PtRe(\mu\text{-}CO)Cl_2(N_2R)(\mu\text{-dppm})_2]$ | Binuclear | 2.859(4)[d] | | 82 |
| **23** | $[PtRe_2(\mu_3\text{-}CC)(CO)_9(PPh_3)_2]$ | See text | 2.731(1) | | 93 |
| **16** | $[PtRe_2(CO)_{12}]$ | Linear | 2.8309(5) | | 84 |
| **18a** | $[PtRe_2(\mu\text{-}H)_2(CO)_8(PPh_3)_2]$ | Triangle | 2.788(1)<br>2.906(1)[c] | 3.203(1) | 85 |
| **19** | $[PtRe_2(\mu\text{-}H)_2(CO)_8(COD)]$ | Triangle | 2.741(1)<br>2.895(1)[c] | 3.115(1) | 87 |
| **21b** | $[PtRe_2(\mu\text{-}H)(\mu\text{-}PPr_2)(CO)_8(PPh_3)_2]$ | Triangle | 2.774(1)[c]<br>2.834(1)[b] | 3.176(1) | 91 |
| **24** | $[PtRe_2\{\mu\text{-}PC(CO)tBu\}(CO)_8(dppe)]$ | See text | — | 3.044(1) | 94 |
| **25** | $[PtRe_3(\mu\text{-}H)_3(CO)_{14}]$ | Spiked triangle | 2.776(1)<br>2.934(1)[c]<br>3.067(1)[c] | 3.152(1) | 87 |
| **28** | $[PtRe_3(\mu\text{-}H)(CO)_{13}]^{2-}$ | Pseudoraft | 2.706(1)<br>2.798(2)<br>2.799(1)[c] | 3.046(1)<br>3.091(1) | 99 |
| **26** | $[PtRe_4(\mu\text{-}H)_6(CO)_{16}]$ | Bow-tie | 2.901(1)[c]<br>2.911(1)[c] | 3.192(1)[c] | 86 |
| **27** | $[PtRe_4(\mu\text{-}H)_5(CO)_{16}]^-$ | Bow-tie | 2.786(1)<br>2.888(1)[c]<br>2.859(1)[c]<br>2.853(1)[c] | 3.168(1)[c]<br>3.147(1)[c] | 86 |
| **29** | $[PtRe_4(CO)_{17}]^{2-}$ | Pseudoraft | 2.7354(8)<br>2.7428(9)<br>2.7583(8)<br>2.7640(8) | 3.0115(9)<br>3.0351(9)<br>3.0495(8) | 99 |
| **33** | $[Pt_2Re_2(\mu\text{-}CO)_4(CO)_6(PPh_3)_2]^e$ | Butterfly | 2.734(1)[d]<br>2.745(1)[d]<br>2.750(1)[d]<br>2.751(1)[d] | 3.094(1) | 88 |
| **35** | $[Pt_2Re_2(\mu\text{-}CO)_4(CO)_6(PCy_3)_2]^f$ | Butterfly | 2.7343(9)[d]<br>2.742(1)[d]<br>2.7473(8)[d]<br>2.756(1)[d] | 3.0560(9) | 91 |
| **36** | $[Pt_2Re_2(\mu\text{-}H)(\mu\text{-}CO)_2(\mu\text{-}PPh_2)\text{-}(CO)_6(PCy_3)_2]^g$ | Butterfly | 2.748(2)[d]<br>2.750(2)[d]<br>2.761(2)[c]<br>2.813(2)[b] | 3.149(2) | 91 |
| **37** | $[Pt_2Re_2(\mu\text{-}CO)_2(C)_6(\mu\text{-dppm})_2]^h$ | Diamond | 2.7994(9)<br>2.7281(9)[d] | | 103 |
| **38** | $[Pt_3Re(CO)_3(\mu\text{-dppm})_3]^+$ | Tetrahedral | 2.649(1)<br>2.684(1)<br>2.685(1) | | 107 |
| **43** | $[Pt_3Re(CO)_3(\mu_3\text{-}O)_2(\mu\text{-dppm})_3]^+$ | See text | 2.843(1)<br>2.854(1) | | 107 |

Table 7 (*continued*)

| Entry | Cluster | Geometry | Pt–Re[a] | Re–Re[a] | Ref. |
|---|---|---|---|---|---|
| 45 | $[Pt_3(ReO_3)(\mu\text{-dppm})_3]^+$ | Tetrahedral | 2.711(3)<br>2.720(3)<br>2.748(1) | | 110 |
| 47 | $[Pt_3Re(CO)_3(\mu_3\text{-}S)_2(\mu\text{-dppm})_3]$ | See text | 2.946(2)<br>3.002(2) | | 111 |
| 34 | $[Pt_3Re_2(\mu\text{-}CO)_6(CO)_4(PPh_3)_3]$[i] | Trigonal bipyramidal | 2.719(2)[d]<br>2.732(2)[d]<br>2.747(2)[d]<br>2.748(2)[d]<br>2.778(2)[d]<br>2.779(2)[d] | 3.237(2) | 88 |

[a] In Å. [b] Bridged by $PR_2$. [c] Bridged by H. [d] Bridged by CO. [e] Pt–Pt = 2.982(1) Å. [f] Pt–Pt = 3.0417(8) Å. [g] Pt–Pt = 3.159(2) Å. [h] Pt–Pt = 2.671(1) Å. [i] Pt–Pt = 2.955(2), 3.009(2) Å.

### 3.2. Synthesis by oxidative addition to Pt(0)

In this approach, a metal complex is oxidatively added to a Pt(0) centre. Thus, when $[CpReH_2(CO)_2]$ is treated with $[Pt(C_2H_4)(PPh_3)_2]$, oxidative addition of the rhenium hydride to the platinum centre takes place, yielding a binuclear complex **6** [70]. The driving force of this process stems in part from the formation of a Pt Re bond. This bond distance has been determined to be 2.838(1) Å, which is slightly longer than unsuppported Pt–Re bonds in other clusters. Important metal–metal distances, along with metal core shapes, of all the Pt–Re clusters can be found in Table 7. In complex **6**, one hydride ligand is believed to be as a terminal PtH and the other as a PtRe($\mu$-H) group. However, the two hydrides are equivalent even at 162 K in the $^1H$ NMR spectra. Since the two phosphines remain inequivalent, a possible explanation of the hydride exchange involves an equilibrium between a $(\mu\text{-H})_2$ structure, **7**, and complex **6** (Scheme 6). The formation of **6** is reversible. So, in the presence of ethylene, the Pt–Re bond of **6** is cleaved and the starting complexes are regenerated. On the other hand, in the presence of both ethylene and hydrogen, complex **6** acts as a catalyst for the hydrogenation of ethylene [71]. Since the rhenium dihydride and the platinum-ethylene complexes, when acting alone, show no or extremely slow hydrogenation activity under similar conditions, the binuclear centre of **6** appears to be involved in the catalytic hydrogenation. A possible mecha-


6 7

Scheme 6. (L = $PPh_3$).

nism involves the insertion of ethylene into the Pt–H bond, followed by reductive elimination of ethane at the platinum centre.

Complex **6** also reacts with alkynes, leading to the fragmentation of the binuclear framework [71,72a]. Thus, when **6** is treated with 2-butyne, a Re-alkene complex, **8**, is formed. The reaction is believed to proceed as shown in Scheme 7, in which the alkyne adds to platinum followed by insertion into the Pt–H bond to give a vinyl species, which then transfers to the rhenium centre. Further evidence in support of the mechanism arises from the reaction of $[Pt\{(E\text{–}C(Me)=CHMe\}L_3]^+$ $(L=PPh_3)$ with $[CpReH(CO)_2]^-$ to give the same cis product **8** [72a]. These reactions have been shown to be stereospecific (for example, **8** can be isolated in 98% yield) and they illustrate a cooperative effect between the two metal centres. A similar reaction of $[Pt\{(E\text{–}C(Me)=CHMe\}L_2]^+$ $(L=PPh_3)$ with $[CpReMe(CO)_2]^-$ leads to a methylene-bridged complex, $[Cp(CO)_2Re(\mu\text{-}CH_2)PtL_2]$, which may be formed by insertion of Pt into a C–H bond, followed by reductive elimination of an olefin molecule. The complex is isoelectronic to complex **6** and contains a 2.730(1) Å Pt–Re bond, shorter than that found for **6** [72b].

Complexes containing secondary phosphine ligands are able to oxidatively

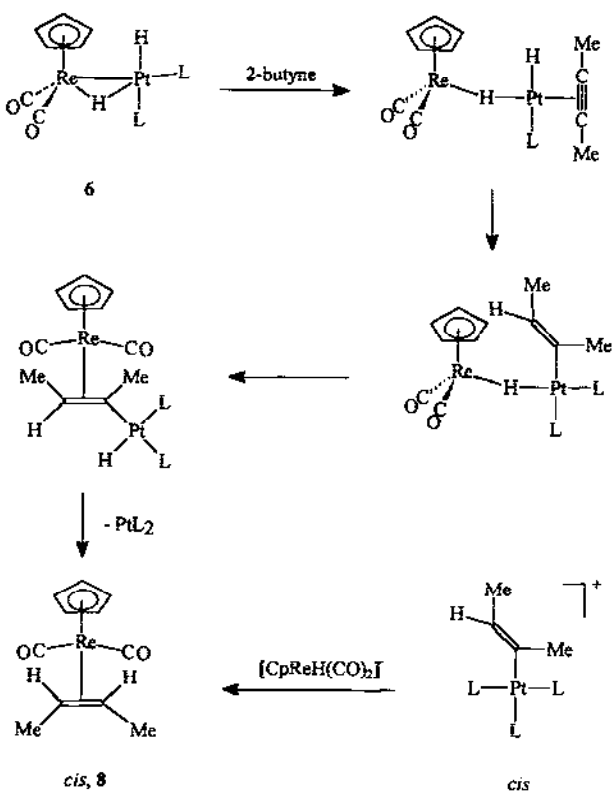


Scheme 7. $(L=PPh_3)$.

add a P–H bond to a Pt(0) centre [73–75]. Scheme 8 shows the reaction of $[CpRe(NO)(CO)(PR_2H)]$ with two platinum complexes [74]. The reaction of $[Pt(C_2H_4)(PPh_3)_2]$ leads to the formation of the phosphido-bridged complex **9**. The spectroscopic data of the complex are similar to those observed for $[PtH(PR_3)_3]^+$, suggesting that the positive charge may be located on the Pt centre. Thus if platinum retains a 16-electron configuration, no Pt–Re bond is expected for **9**. In contrast, the reaction of $[Pt(PPh_3)_4]$ is accompanied by rapid CO loss, yielding complex **10** that contains a Pt–Re bond. Upon standing, the terminal-hydride complex **10** rearranges to the bridging-hydride complex **11**. This isomerization reaction is catalyzed by halide and pseudohalide ions, with $N_3^-$ and $F^-$ being most and least effective, respectively. The mechanism of the catalytic isomerization may involve the attack of the halide anion at both the platinum and rhenium centres, and subsequent bridging by the hydride and loss of the halide ion give complex **11**. Complex **9** is relatively stable with respect to CO loss. However, in the presence of bases such as $F^-$ or proton sponge, **9** can be readily converted to **10**. Since thermal CO loss from the 18-electron complexes $[CpRe(NO)(CO)L]$ is notably difficult [76], the substitution of CO from $[CpRe(NO)(CO)(PR_2H)]$ on the formation of **11** is significant. Detailed study indicates that this process involves the transfer of CO from the rhenium centre to the platinum atom, via $\mu$-CO, to give complex **12**. Addition of a phosphine to the Pt centre in **12** gives rise to the rapid formation of **11**, accompanied by the CO loss (Scheme 9). In complex **12**, the platinum has a 16-electron configuration, so CO substitution can be expected to occur easily via an associative pathway. The transformation from **9** to **11**, together with that shown in Scheme 7 and those to be discussed below, illustrates that ligand transfer could easily take place between platinum and rhenium. The structures of **10b** (R = Cy), **11a** (R = Ph) and **11b** (R = Cy) have been determined. The geometries of the three complexes are very similar except that there is a bridging hydride in **11**. The Pt–Re bond distances ranges from

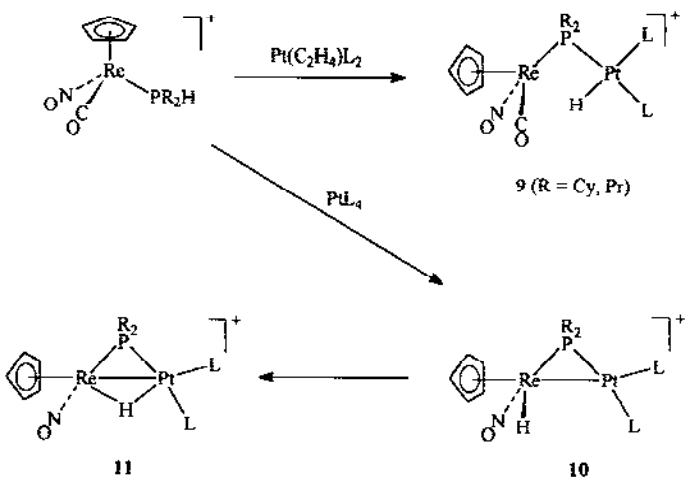


Scheme 8. (L = $PPh_3$, R = Ph, a; Cy, b; Pr, c).

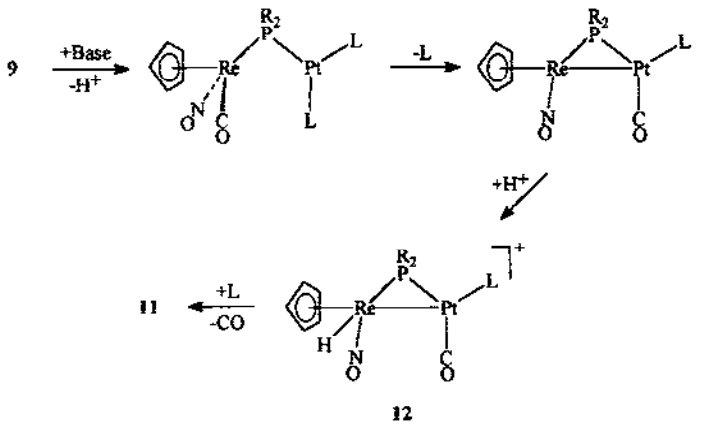

Scheme 9.

2.8673 (4) to 2.8815 (8) Å, and moving the terminal hydride in **10b** to the bridging position in **11b** does not lengthen the Pt–Re bond [2.8675(5) vs. 2.8673(4) Å]. For either the terminal or the bridging phosphine ligands, the Pt–P bond distances of the three complexes correlate well with observed $^1J$(Pt–P) values, as has been observed for several other complexes [77,78].

The complex $[Pt(C_2H_4)(PPh_3)_2]$ reacts with $[ReX(CO)_5]$ (X= Br, H) and, at room temperature, the reaction leads rapidly to $CO/PPh_3$ exchange between the Pt and the Re complexes (Scheme 10) [79]. However, at lower temperature the reaction affords, reversibly, a binuclear complex, **13**, which was characterized spectroscopically. The structure of $[(CO)_4Mn(\mu\text{-}H)(\mu\text{-}CO)Pt(PEt_3)_2]$, a manganese analogue of **13**, has been determined [80], providing credence to the suggested structure of **13**. Variable-temperature NMR spectra indicate that **13** (X=H) is fluxional. One exchange process makes the four CO ligands cis to the bridging hydride equivalent, and a second exchange process makes the two phosphine ligands equivalent. Upon raising the temperature, complex **13** decomposes to give the same products obtained at room temperature. However, a kinetic study shows that **13** is not an intermediate in the reaction at room temperature. Interestingly, the complex $[Pt(C_2H_4)(PPh_3)_2]$

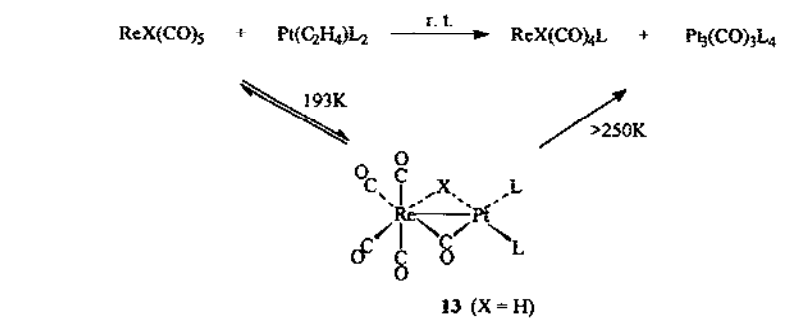

Scheme 10. (X=H, Br, L=$PPh_3$).

is found to catalyze the substitution of CO by phosphine in $[ReBr(CO)_5]$ to give *cis*-$[ReBr(CO)_4(PPh_3)]$. In the absence of the Pt complex the substitution is slower, and a mixture of mono- and di-substitution products are obtained [79]. A similar effect has been reported for $[Pt(PPh_3)_4]$, which catalyzes the substitution of CO by $PR_3$ in some carbonyl complexes [81]. These reactions demonstrate again that Pt is able to facilitate CO labilization of normally inert Re–CO bonds. The mechanism of the reactions may involve intermediates similar to **13** and those shown in Scheme 9.

### 3.3. Other synthetic methods

Binuclear Pt–Re complexes have also been prepared by using a ring-opening method. Thus, when $[ReCl(CO)(N_2R)(diphosphine\text{-}PP')(diphosphine\text{-}P)]^+$ (R = $C_6H_4Me$-4), which contains a chelated and a dangling diphosphine ligand, is refluxed with $[PtHCl(PPh_3)_2]$, complex **14** is formed as shown in Scheme 11. The Pt–Re bond distance in **14a** is 2.859(4) Å, the carbonyl ligand is semibridging with the angle Re–C–O = 158.4°. The angles C–N–N = 119(1)° and Re–N–N = 164(1)° are indicative of a singly bent 3-electron diazenido ligand [82] and, as expected, complex **14b** undergoes electrophilic reaction at the $N_\beta$ of the diazenido ligand to form complex **15** (R' = H, Me). A number of heterobinuclear complexes have been prepared using the diphosphine ring opening strategy used to prepare **14** [83].

## 4. Pt–Re clusters of higher nuclearity

These clusters will be treated according to the number of platinum atoms contained. There are Pt–Re clusters known with one, two or three platinum atoms. With one platinum atom, there may be 2,3,4 or 7 Re atoms; with two platinum

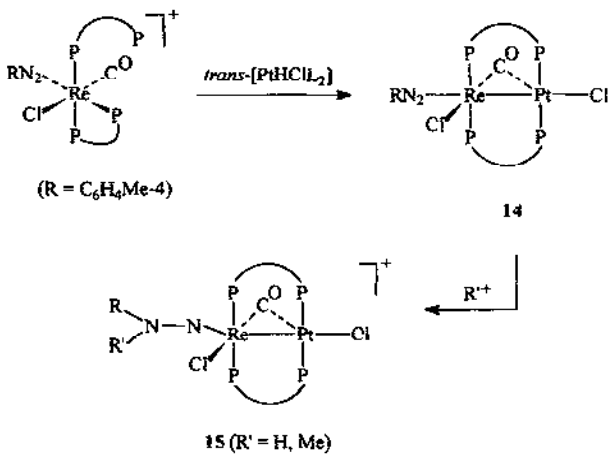


Scheme 11. (**a**, P^P = $Ph_2PCH_2PPh_2$ = dppm; **b**, P^P = $Ph_2PC(=CH_2)PPh_2$).

atoms, only $Pt_2Re_2$ clusters are known, and with three platinum atoms there may be 1 or 2 Re atoms.

### 4.1. Complexes containing one platinum atom

#### 4.1.1. $PtRe_2$ clusters

As with the synthesis of binuclear Pt–Re complexes, Pt(0) complexes prove to be the most versatile building fragments toward Pt–Re clusters of higher nuclearity. The earliest Pt–Re cluster appears to be the linear complex $[PtRe_2(CO)_{12}]$, **16**, prepared by the reaction of $[PtMe_2(COD)]$ with $[HRe(CO)_5]$ in the presence of CO [84]. An earlier report mentioned the cluster $[PtRe_2H_2(PPh_3)(CO)_9]$, but details are not available [69]. Structure determination shows that **16** possesses $D_{2h}$ symmetry, with the Re–Pt–Re angle = 180°. The four carbonyls on one rhenium are eclipsed relative to the carbonyls on the other rhenium, but staggered relative to the carbonyls on platinum. Other $PtM_2$ compounds having a linear metal core structure are also known; an example reminiscent of **16** is $[PtMn_2(CO)_{10}(py)_2]$. The formation of **16** proceeds via elimination of methane. Similar reactions of metal alkyls with hydrides, via reductive elimination of alkanes, have led to the preparation of other cluster complexes [64].

Many Pt–Re clusters have been synthesized by the use of binuclear hydrido rhenium carbonyl complexes [85–88]. Thus, when the unsaturated complex $[Re_2(\mu\text{-}H)_2(CO)_8]$ is treated with $[Pt(C_2H_4)(PPh_3)_2]$ at low temperature, insertion of the $[Pt(PPh_3)_2]$ fragment into a $Re(\mu\text{-}H)Re$ linkage takes place to give the 46-electron complex **17**, which rearranges to **18** at room temperature, via exchange of a phosphine and a CO ligand between platinum and one of the rhenium centres (Scheme 12) [85]. The complex $[Re_2(\mu\text{-}H)_2(CO)_8]$, which contains a Re–Re double bond, is ethylene-like, and the fragment $[Pt(PPh_3)_2]$ is isolobal to $CH_2$, so the ready formation of the metallocyclopropane complex **17** is not surprising, and is analogous to the preparation of **1** from alkylidenes. In solution, **18** exists as two interconverting isomers, **18a** and **18b**, with the former being the major species; its structure has been determined by X-ray diffraction. These complexes exhibit complicated dynamic behaviour in solution, as shown by variable-temperature NMR experiments and $^{31}P$ 2D exchange spectroscopy [89]. There are two exchange processes for **17**, the first one, operating at lower temperature, involves the hopping of the bridging hydride from one Pt–Re edge to the other, while the second one, observable at higher temperature, involves the transfer of the hydride bridging the Re–Re edge to a Pt–Re edge, accompanied by a simultaneous shift of the hydride at the Pt–Re edge to the

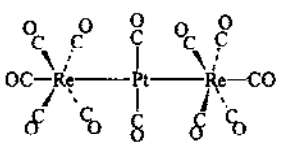


**16**

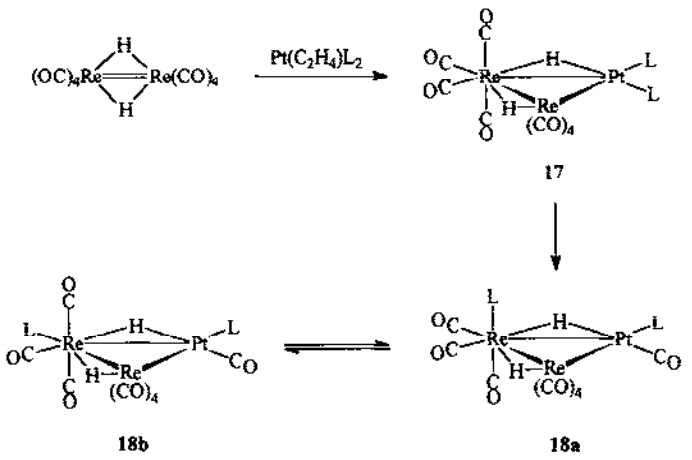


Scheme 12. (L = $PPh_3$).

Re–Re edge. Besides the isomerization, the CO ligands on the $Re(CO)_3(PPh_3)$ moiety in **18a** also undergo a scrambling process.

The two Pt–Re bond distances in **18a** are quite different, 2.788(1) vs 2.906(1) Å, with the longer distance assigned to the bridging hydride. The exchange of CO and $PPh_3$ between Pt and Re on going from **17** to **18** takes place easily, as judged by the low activation energy of about 80 kJ $mol^{-1}$, and so represents another example of Pt–assisted CO labilization in the Pt–Re system.

In a similar reaction, the complex $[Re_2(\mu\text{-}H)_2(CO)_8]$ is treated with $[Pt(COD)_2]$ to form complex **19**. The weakly coordinating COD in **19** can replaced by a phosphine ligand to give complex **17** (Scheme 13) [86,87]. In **17** and **19**, the Pt–Re bond has been found to have a higher trans influence than the Pt($\mu$-H)Re moiety [79,85,87,90]. Thus, in **19** the Pt–C bonds trans to Re are over 0.1 Å longer than the Pt–C bonds trans to hydride, and, in **17**, the phosphorus trans to Re displays a much smaller $^1J$(PtP) (2167 Hz) than the one trans to hydride (4142 Hz). A marked difference in $^1J$(PtP) is also observed in complex **13**, with the phosphine trans to the CO ligand displaying a much smaller $^1J$(PtP) than that trans to the hydride, suggesting that the trans influence of the bridging hydride is also smaller than that of a bridging CO ligand [79].

The cluster $[PtRe_2(CO)_{10}(PCy_3)]$, **20** is obtained by reaction of $[Pt(C_2H_4)_2(PCy_3)]$ with $[Re_2(CO)_{10}]$ [91]. In this reaction, the PtL unit adds to

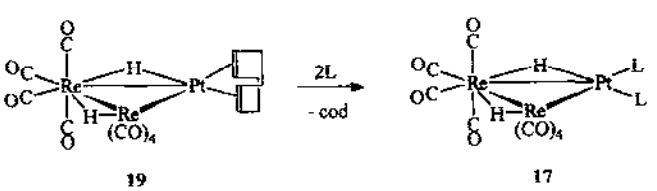


Scheme 13. (L = $PPh_3$).

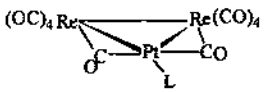

**20** (L = $PCy_3$).

the Re–Re bond of $[Re_2(CO)_{10}]$ and **20** can add a second PtL unit to give a $Pt_2Re_2$ cluster, which is described in Section 4.2.

Reaction of $[Pt(C_2H_4)(PPh_3)_2]$ with $[Re_2(CO)_9(PR_2H)]$ at room temperature gives the trinuclear cluster, **21**, with loss of CO (Scheme 14) [91]. For the complex $[Re_2(CO)_9(PR_2H)]$, CO substitution is difficult and occurs only when the complex is heated at 170 °C, yielding a $\mu$-phosphido-$\mu$-hydrido complex, $[Re_2(\mu\text{-H})(\mu\text{-PR}_2)(CO)_8]$ [91]. Thus, the easy reaction leading to **21** provides yet another example of platinum-assisted CO labilization. As with the reaction in Scheme 8, the mechanism accounting for this labilization process involves the oxidative addition of the P–H bond at the platinum centre, followed by CO transfer, via a $\mu$-CO group, from rhenium to platinum, whereupon CO dissociation and Pt–Re bond formation take place.

On the other hand, when $[Re_2(CO)_9(PPh_2H)]$ is reacted with $[Pt(C_2H_4)_2(PCy_3)]$, a different cluster **22**, is formed, in which a phosphide ligand bridges the Re–Re bond, and there are still nine CO ligands with one of them bridging a Pt–Re edge (Scheme 14) [91]. The formation of **22** instead of **21** may be due to the steric bulkiness of the $PCy_3$ ligands, which could force the phosphido ligand to rearrange from bridging a Pt–Re bond to bridging the Re–Re bond in **22**. This explanation assumes that the oxidative addition of the P–H bond at platinum is the first step.

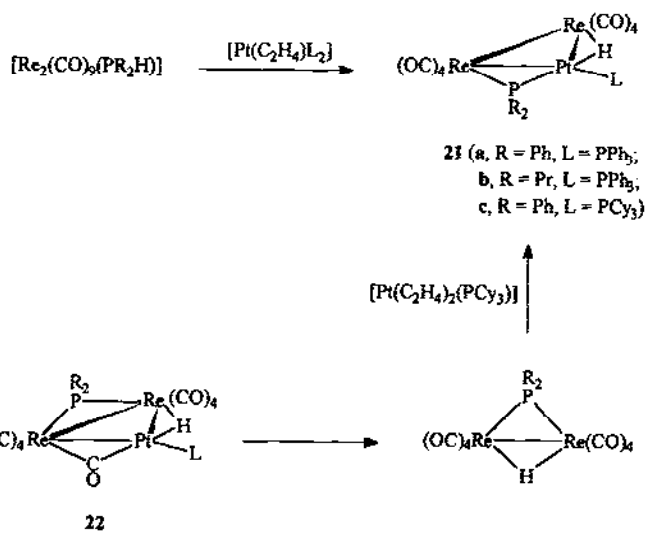

**21** (a, R = Ph, L = $PPh_3$;
b, R = Pr, L = $PPh_3$;
c, R = Ph, L = $PCy_3$)

**22**

Scheme 14.

On standing, complex **22** decomposes to give $[Re_2(\mu\text{-}H)(\mu\text{-}PPh_2)(CO)_8]$ and $[Pt_3(\mu\text{-}CO)_3(PCy_3)_3]$. When $[Pt(C_2H_4)_2(PCy_3)]$ is reacted with $[Re_2(\mu\text{-}H)(\mu\text{-}PPh_2)(CO)_8]$, cluster **21c** is generated, in which the $PPh_2$ ligand bridges the Pt–Re bond. The migration of the bridging $PPh_2$ unit from an Re–Re to a Pt–Re edge is again necessary for this transformation.

Platinum(0) complexes react readily with organic alkynes [92]. The same is also true with the reaction between $[Pt(C_2H_4)(PPh_3)_2]$ and a dimetallated alkyne, $[(OC)_5ReCCRe(CO)_5]$, yielding an acetylide-bridged complex, 23 [93]. The Pt–Re bond distance [2.731(1) Å] of **23** is shorter than those found in most Pt–Re clusters (Table 7). Complex **23** may be considered as a Pt–Re binuclear compound, with the second Re centre appended, since there is only one metal–metal bond.

The unsaturated complex $[Re_2H_2(CO)_8]$ is shown to react with a phospha-alkyne complex, [Pt(dppe)($^t$BuCP)], to give cluster **24**, the $^t$BuC(CO)P moiety of which results from CO attack at the $^t$BuC≡P ligand [94]. The phosphorus atom in **24** is in bonding distance of all three metal atoms and so the novel phosphide may be considered as a 4-electron ligand.

*4.1.2. $PtRe_3$-$PtRe_7$ clusters*

Remarkably, the platinum centre in $[PtRe_2(\mu\text{-}H)_2(CO)_8(COD)]$, **19**, is subject to attack by $[HRe(CO)_5]$ and $[Re_2(\mu\text{-}H)_2(CO)_8]$ (Scheme 15) [86,87]. Thus, when treated with $[HRe(CO)_5]$ in the presence of CO, the triangular cluster **19** is converted to a spiked triangular $PtRe_3$ complex, **25**. The overall reaction leads to replacement of the COD ligand in **19** by a CO ligand and a $[HRe(CO)_5]$ molecule [87]. Reacting **19** with CO at low temperature also gives this complex, but at room temperature $[PtRe(CO)_{12}]$, **16**, is formed. In complex **25**, neither the CO ligand nor the rhenium hydride fragment could be replaced by the other to form a bis substituted product. The $[HRe(CO)_5]$ molecule is suggested to act as a two electron donor and, together with the CO, this provides the platinum atom with a **16** electron configuration. Since it was not possible to prepare a bis substituted cluster by displacement of COD by two $[ReH(CO)_5]$ molecules, the addition of CO appears to be necessary to form a stable complex. The $[HRe(CO)_5]$ unit is also observed in the L-shaped complexes $[Mn_2Re(\mu\text{-}H)(CO)_{14}]$ [95] and $[Re_3(\mu\text{-}H)(CO)_{14}]$ [96], where it can be viewed as a two electron donor that substituted a CO ligand from the binuclear $[M_2(CO)_{10}]$.

The COD ligand is replaced when **19** is reacted with $[Re_2(\mu\text{-}H)_2(CO)_8]$, resulting

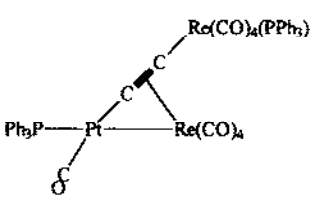


23

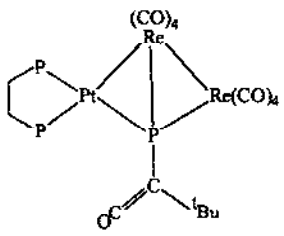


24

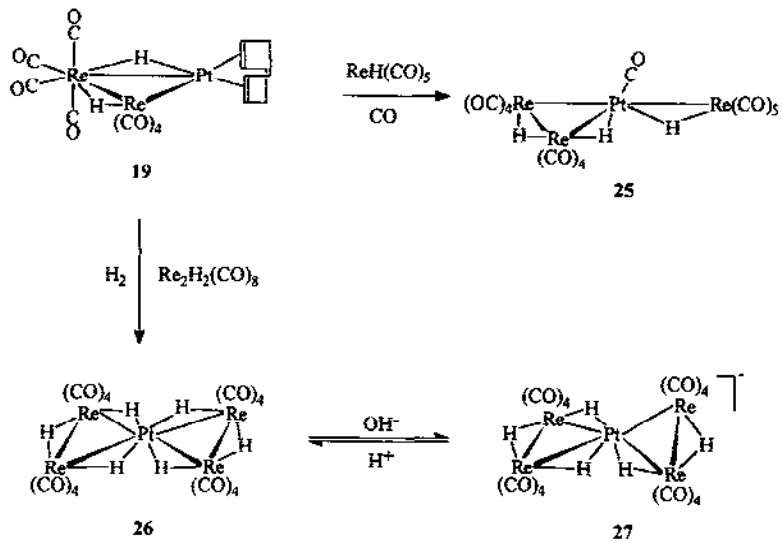


19 25 26 27

Scheme 15.

in the formation of the bow-tie pentanuclear $PtRe_4$ cluster **26** [86]. This reaction requires the presence of $H_2$, which plays a role similar to CO in the formation of **25**. In the presence of $OH^-$, **26** is further converted to its conjugate base, cluster **27**. This reaction is reversible. The complex $[Re_2(\mu\text{-}H)_2(CO)_8]$ also adds $[Ir(CO)_4]^-$ to give interesting clusters such as $[\{IrRe_2(\mu\text{-}H)(CO)_{11}\}_2]^{2-}$, in which two $Re_2Ir$ triangles are joined by an Ir–Ir bond [97].

The structures of complexes **19** and **25–27** have all been determined by X-ray diffraction. In **25**, the rhenium attached to the $PtRe_2$ triangle is significantly displaced out of the triangular plane (about 1.1 Å) [87], and while **26** possesses a planar geometry, this planarity is lost when it is deprotonated to give **27**, in which the two triangles have a dihedral angle of 36.3° [86]. As with complex **18a**, the two Pt–Re bond distances within each triangle of these clusters are different, with the hydride-bridged edge being significantly longer (by ca. 0.07–0.16 Å) than the unbridged edge. Complex **26** has 76 CVEs, as expected for a pentanuclear cluster containing a planar platinum centre. The electron count for **27** is the same and the reason for the larger deviation from planarity is not obvious. In solution, complex **25** exists as two isomers, resulting from a dynamic process involving hopping of the hydride from one Pt–Re edge to the other within the triangle [98]. Interestingly, $^1H$ 2D EXSY experiments also reveal an intermolecular process operating for only one of the isomers. This process involves the exchange of the $[ReH(CO)_5]$ moiety between molecules of the same kind, and so, as expected, addition of free $[ReH(CO)_5]$ caused a strong increase in the exchange rate. A similar process has been reported for the L-shaped complex $[Mn_2Re(\mu\text{-}H)(CO)_{14}]$ and $[ReH(CO)_5]$, which slowly reaches equilibrium with $[Re_2Mn(\mu\text{-}H)(CO)_{14}]$ and $[MnH(CO)_5]$ [95].

Condensation of $[\{Pt_3(CO)_6\}_n]^{2-}$ with $[Re_2(\mu\text{-}H)H_2(CO)_8]^-$ yields a tetranuclear

$PtRe_3$ cluster, **28**, while the reaction of the same platinum anion with $[Re(CO)_5]^-$ gives a pentanuclear $PtRe_4$ cluster, **29**. Cluster **29** may also be obtained by treating $[PtCl_2(NCPh)_2]$ with four equivalents of $[Re(CO)_5]^-$ [99]. In the two complexes, the triangles are not co-planar, so they are pseudo-raft in geometry. The Pt–Re bond separations range from 2.706(1) to 2.799(1) Å, with the hydride-bridged Pt–Re edge being the longest. The Re–Re bond distances ranges from 3.0115(9) to 3.091(1) Å, notably shorter than the hydride-bridged Re–Re distances in complexes mentioned earlier (see Table 7). Cluster **29** may be considered to be formed from **28** by replacement of the bridging hydride ligand by a $Re(CO)_4$ group. The nuclearity of **28** and **29** is the same as that of **25** and **26** but the electron counts and hence the number of metal–metal bonds differ.

The largest known Pt–Re clusters are the $PtRe_7$ complexes **30** and **31**, prepared by the reaction of $[Re_7C(CO)_{21}]^{3-}$, **32**, with $[Pt(\eta_3\text{-}C_4H_7)Cl]^2$ and $[PtMe_3I]_4$ respectively [100,101]. These clusters can be related to the complexes CpMLn, $[CpPt(\eta^3\text{-allyl})]$ and $[CpPtMe_3]$, if the anion $[Re_7C(CO)_{21}]^{3-}$ is considered isolobal to the $C_5H_5^-$ ligand (100).

### 4.2. Complexes containing two platinum atoms

The reaction of $[Pt(C_2H_4)(PPh_3)_2]$ with $[Re_2(CO)_{10}]$ at room temperature gives the clusters $[Pt_2Re_2(CO)_{10}(PPh_3)_2]$, **33**, and $[Pt_3Re_2(CO)_{10}(PPh_3)_3]$, **34**, with the former being the major product [88]. The formation of **33** and **34** can be viewed to

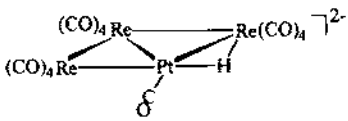


**28**

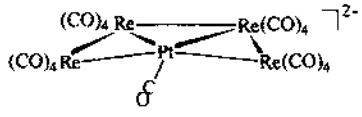


**29**

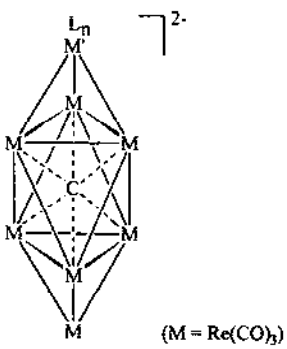


(M = $Re(CO)_3$)

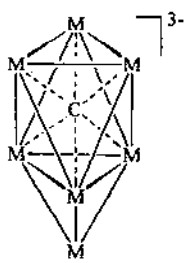


**32**

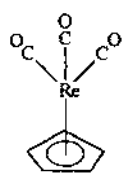


**30** ($M'L_n = PtC_4H_7$)

**31** ($M'L_n = PtMe_3$)

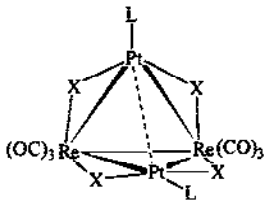


33 (X = CO, L = $PPh_3$).

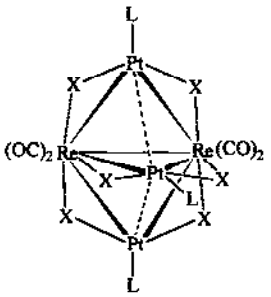


34 (X = CO, L = $PPh_3$).

involve sequential edge capping of the Re–Re bond of $[Re_2(CO)_{10}]$ by two and then three $Pt(PPh_3)$ fragments. The reaction proceeds via an intermediate, which may be the first number of this class of clusters, namely $[PtRe_2(CO)_{10}(PPh_3)]$. The cluster $[Pt_2Re_2(CO)_{10}(PCy_3)_2]$, **35**, is obtained in a similar way by reaction of $[Pt(C_2H_4)_2(PCy_3)]$ with $[Re_2(CO)_{10}]$ [91]. In this case, IR monitoring indicates the rapid and quantitative formation of an intermediate cluster $[PtRe_2(CO)_{10}(PCy_3)]$, **20**, which is then converted to **35** on addition of a further mole of $[Pt(C_2H_4)_2(PCy_3)]$. Complexes **33** and **35** are approximately tetrahedral, while **34** is approximately trigonal bipyramidal. The Re–Re distances of 3.094(1) Å in 33 and 3.0560(9) Å in **35** are in the single bond region (comparable to those observed for **28** and **29** for example), but adding one more $Pt(PPh_3)$ unit to the Re–Re hinge, resulting in the formation of **34**, leads to a significant increase in the Re–Re separation to 3.237(2) Å. The Pt–Re bond distances (av. 2.745 in **33**, 2.751 Å in **34**, 2.745 Å in **35**) in the clusters are markedly shorter than the hydride-bridged Pt–Re edges in clusters such as **19** and **25–27**, and also shorter than some of the unsupported Pt–Re bonds such as those in **6**, **16** and **18a**. This appears to agree with a previous observation that CO bridged M–M bonds are often shorter than the unbridged M–M bonds, whereas bridging hydride tends to lengthen such bonds [102]. The Pt...Pt separations, ranging from 2.955 to 3.009 Å in **33–35** are nonbonding or borderline and so **33** and **35** may be better described as butterfly clusters. Complexes **33** and **34** have 58 and 70 CVEs respectively and, if the platinum centres adopt a 16-electron configuration, theory would suggest that the Pt...Pt separations in **33–35** should be viewed as non-bonding.

The 58-electron cluster $[Pt_2Re_2(CO)_8(\mu\text{-}H)(\mu\text{-}PPh_2)(PCy_3)_2]$, **36**, is isolated after prolonged reaction of $[Pt(C_2H_4)_2(PCy_3)]$ with $[Re_2(CO)_9(PPh_2H)]$ and is probably formed from the $PtRe_2$ cluster **21c** by reaction with $[Pt(C_2H_4)_2(PCy_3)]$ [91]. Cluster **36** has a butterfly structure, and is related to **33** and **35** by replacement of two bridging CO ligands in the latter by a $\mu$-H and $\mu$-$PPh_2$ unit. The Pt...Pt separation of 3.159(2) Å in **36** suggests that no Pt–Pt bonding is present. In both complexes **21b** and **36**, the hydride-bridged Pt–Re bonds [2.774(1) and 2.761(2) Å] are shorter than the Pt($\mu$-$PR_2$)Re edges [2.834(1) and 2.813(2) Å], and are longer than the CO-bridged Pt–Re bonds in **33–36** (av. ca. 2.75 Å).

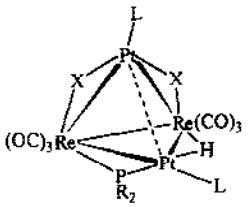

**36** ( R = Ph, L = $PCy_3$)

Another 58-electron $Pt_2Re_2$ cluster is the diamond cluster $[Pt_2Re_2(CO)_8(\mu\text{-dppm})_2]$, **37** (dppm = $Ph_2PCH_2PPh_2$), which contains a Pt–Pt bond of 2.671(1) Å, and is strictly planar (Scheme 16) [103]. In **37** each metal centre has its preferred electron count, that is 16 for Pt and 18 for Re. The Re...Re distance of 4.840(1) Å in **37** is clearly non-bonding. The marked difference between the structures of **37** and **33–36** is believed to stem from the influence of the supporting ligands. While a tetrahedral or butterfly core may be stable with the monodentate CO and $PR_3$ ligands, a planar geometry is more compatible with the bridging dppm ligands. The result is that in **33–36** there is no Pt..Pt bond whereas in **37** there is no Re..Re bond. A related case of cluster isomerism is in the clusters $[Pt_2Mo_2(Cp)_2(CO)_6(PR_3)_2]$ which can exist in both planar and tetrahedral forms; in this case the steric effects of the ligands determine the preferred structure [104]. Cluster **37** is formed by the reaction of $[Pt_2Cl_2(\mu\text{-dppm})_2]$ with $[Re(CO)_5]^-$ (Scheme 16). The reaction proceeds via two intermediate complexes, which are characterized spectroscopically. The proposed structures are shown in Scheme 16 and are the linear $[Pt_2Re(CO)_6(\mu\text{-dppm})_2][Re(CO)_5]$ and the spiked triangle complex $[Pt_2Re_2(CO)_9(\mu\text{-dppm})_2]$, for

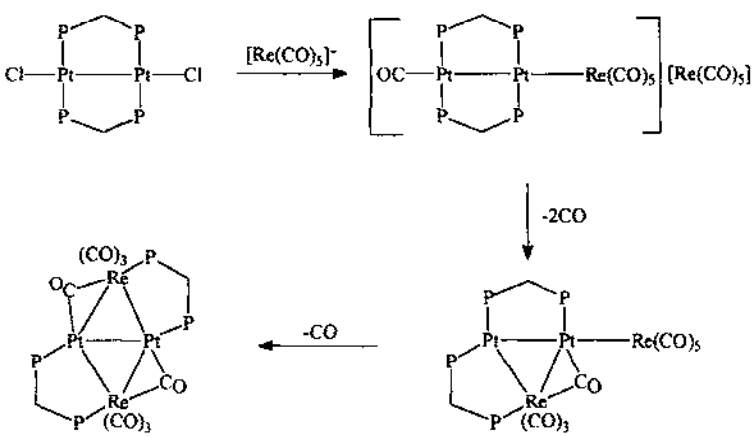

**37**

Scheme 16.

which a close analogue is the cluster $[Pd_2Mn_2(CO)_9(\mu\text{-dppm})_2]$ obtained by reaction of $[Pd_2Cl_2(\mu\text{-dppm})_2]$ with $[Mn(CO)_5]^-$ [105].

### 4.3. Complexes containing three platinum atoms

The cluster $[Pt_3Re_2(CO)_{10}(PPh_3)_3]$, **34**, has already been described in Section 4.2. When $[Pt_3(\mu_3\text{-CO})(\mu\text{-dppm})_3]^{2+}$ [106] is treated with $[Re(CO)_5]^-$, a 54-electron tetrahedral $Pt_3Re$ cluster $[Pt_3\{\mu_3\text{-}Re(CO)_3\}(\mu\text{-dppm})_3]^+$, **38**, is formed. The Mn analogue can be prepared similarly [107,108]. The structure of **38** has been determined and the Pt–Re bond distances, av. 2.673 Å, are the shortest of those reported in Table 7 indicating strong PtRe bonding. The optimum electron count for a tetrahedral cluster in which all metal centres are coordinatively saturated is 60 CVEs. Therefore, **38** is coordinatively unsaturated. In terms of valence bond reasoning, the bonding in **38** can be interpreted as shown in **38b**, that is the three Pt–Re bonds are formed by electron donation from the three Pt–Pt bonds of a $Pt_3(\mu\text{-dppm})_3$ fragment to the three acceptor orbitals of the $[Re(CO)_3]^+$ fragment. In this way, each Pt atom shares 16 electrons and the Re atom shares 18 valence electrons. This simple interpretation is consistent with the result of a molecular orbital calculation [107,108].

The development of Pt–Re clusters has been largely limited to the synthesis of new examples and to studies of structure and bonding, but an extensive chemistry has recently been established for the cluster **38**, including ligand addition, oxidation and sulfidation [107–111]. Scheme 17 summarizes the ligand addition reactions of this cluster [107,109]. Ligand addition occurs at the Re centre for neutral reagents to give **39**, indicating that Re is the major site of coordinative unsaturation. This is perhaps unexpected since the Re centre in **38** has a share of 18 valence electrons, but if ligand addition is accompanied by the scission of one of the Pt–Re bonds, the Re centre can maintain the 18-electron configuration. This weakening of the Pt–Re bond on ligand addition has been confirmed by the structure determination of **39c**, the cluster with $L = P(OPh_3)_3$. For the alkyne adduct, spectroscopic data is consistent with the C–C multiple-bond being parallel to the $Pt_3$ triangle. In contrast, anion

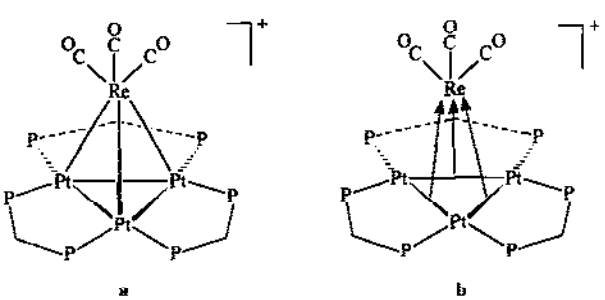


**38** (P^P = dppm)

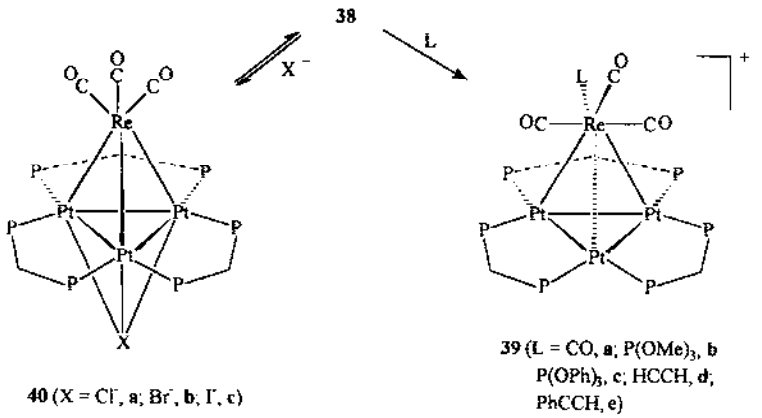


Scheme 17.

additions occur at the other face of the Pt3 triangle to give **40**. The reaction is reversible, with the product being favoured in the order $I^- > Br^- > Cl^-$.

When excess CO is added to **38** in $CH_2Cl_2$, further reaction takes place, leading to the decomposition of the $Pt_3Re$ metal core to give a known cluster cation, $[Pt_3(\mu\text{-}Cl)(\mu_3\text{-}CO)(\mu\text{-}dppm)_3]^+$, **41**, which was previously obtained by treating $[Pt_3(\mu_3\text{-}CO)(\mu\text{-}dppm)_3]^{2+}$ with $Cl^-$. NMR monitoring appears to indicate that the fragmentation proceeds via an intermediate cluster, formed by addition of a second CO to give $[Pt_3\{Re(CO)_5\}(\mu\text{-}dppm)_3]^-$. These reactions can be understood in terms of Scheme 18 [109]. Sequential CO additions at Re give the tetracarbonyl and pentacarbonyl clusters and the next addition occurs at Pt with displacement of $[Re(CO)_5]^-$. The chloro ligand is probably generated by the reaction of $[Re(CO)_5]^-$ with $CH_2Cl_2$.

The reactions shown in Schemes 17 and 18 can be considered analogous to the ligand addition reactions of $[CpRe(CO)_3]$ and the related $[CpRe(CO)(NO)R]$, which result in slippage of the $\eta^5$-$C_5H_5$ ligand to $\eta^3$ and then to $\eta^1$ [112,113]. Hence, the addition of one or two ligands to **38** might lead to slippage of the $Re(CO)_3L_n$ unit from $\eta^3$ ($n=0$) to $\eta^2$ ($n=1$) and $\eta^1$ ($n=2$) with respect to the $Pt_3$ triangle. The similarity in ligand additions between the two different classes of complexes appears not to be accidental. Both the $Pt_3(\mu\text{-}dppm)_3$ fragment and the $C_5H_5^-$ ligand have three donor orbitals of $a_1$ + e symmetry and so, in the limit, cluster **38** can be considered isolobal to $[CpRe(CO)_3]$. It is also interesting to note that, although both $[Pt_3(\mu_3\text{-}CO)(\mu\text{-}dppm)_3]^{2+}$ and cluster **38** are coordinatively unsaturated, the former adds ligands by coordination to one or more platinum atoms while **38** adds ligands at rhenium.

The most remarkable reactions of **38** involve oxidation, using the reagents $Me_3NO$, $O_2$ or $H_2O_2$ [107,110,114]. The reactions occur under mild conditions, affording the series of oxo clusters $[Pt_3\{Re(CO)_3\}(\mu_3\text{-}O)_n(\mu\text{-}dppm)_3]^-$, **42**, $n=1$; **43**, $n=2$; **44**, $n=3$, and at high temperature, the reaction with $O_2$ can also give $[Pt_3(ReO_3)(\mu\text{-}dppm)_3]^+$, **45**, the first example of a cluster containing metals in widely different

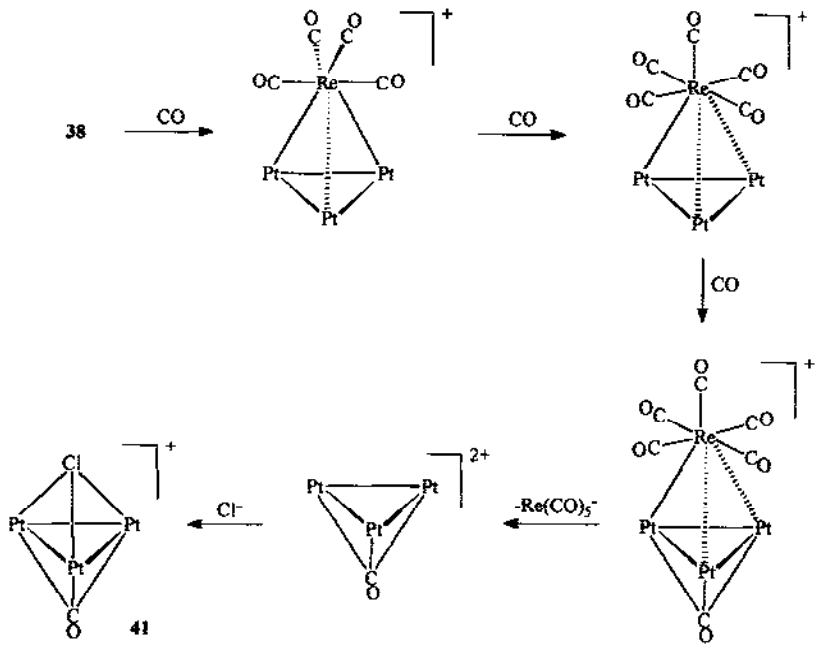


Scheme 18. (dppm ligands omitted).

oxidation states (Scheme 19). The mono-oxo cluster **42** is formed when **38** is treated in a 1:1 molar ratio with $Me_3NO$. Cluster **42** is reactive and is converted to the dioxo cluster **43** upon exposure to further $Me_3NO$ or $O_2$. The dioxo cluster **43** is also obtained directly by the reaction of **38** with $O_2$; in this case, no intermediate is detected by NMR and the reaction appears to mimic dissociative chemisorption of $O_2$ on a metal surface. Thus, this reaction is the first example of oxidative addition of $O_2$ to a metal cluster to give a bis($\mu_3$-O) cluster. The trioxo cluster **44** is readily prepared in high yield by treatment of **38** with $H_2O_2$, and NMR monitoring shows that **43** is an intermediate cluster formed in the course of the oxidation. The cluster **44** could also be generated in good yield by irradiation of a solution of **38** in tetrahydrofuran in the presence of oxygen, a reaction which also involves the intermediacy of **43**. In contrast, the mononuclear complex [$\eta^5$-CpRe(CO)$_3$] yields [$\eta^5$-CpRe(CO)$_2$(THF)] under similar conditions [115] and [($\eta^5$-$C_5Me_5$)Re(CO)$_3$] gives [($\eta^5$-$C_5Me_5$)$ReO_3$] on exhaustive photolysis under an oxygen atmosphere. The conversion of [($\eta^5$-$C_5Me_5$)Re(CO)$_3$] to [($\eta^5$-$C_5Me_5$)$ReO_3$] can also be accomplished using $H_2O_2$ as reagent [116]. In contrast, there is no loss of the coordinated carbonyl ligands in reaction of **38** with $H_2O_2$ or $O_2$/h$\nu$ under the conditions of the study. The novel terminal trioxo cluster **45** is prepared by the reaction of **38** with $O_2$ in refluxing *o*-xylene, again via the intermediacy of **43**. More extended reflux results in further oxidation of **45**[$PF_6$] to give **45**[$ReO_4$]. The [$ReO_4$]$^-$ ion is clearly formed by oxidation of the $Pt_3(ReO_3)$ group in **45**. Perhaps surprisingly, cluster **44** is not detected at intermediate stages of the reaction leading to **45** and attempts to convert

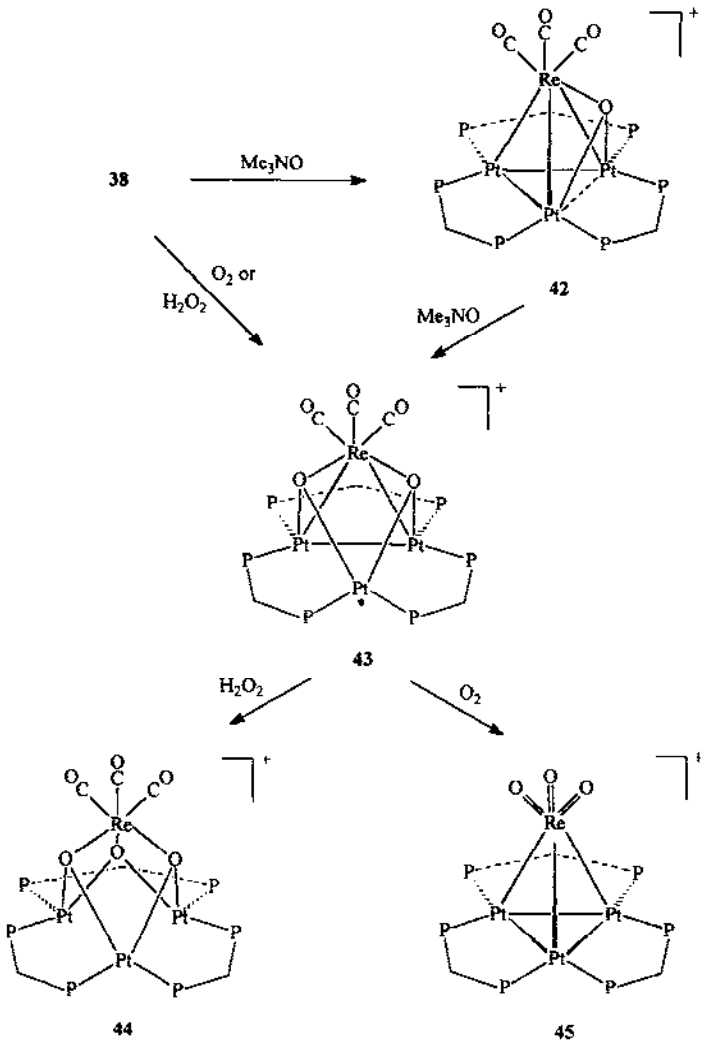


Scheme 19.

**44** to **45** have not been successful. Just as there is an isolobal analogy between **38** and [$\eta^5$-CpRe(CO)$_3$], so there is between **45** and [($\eta^5$-$C_5Me_5$)$ReO_3$]. This series of oxo clusters adds considerably to the small number of known late transition metal oxo clusters [117,118].

In a similar way, the cluster **38** can be sulfided [111]. Thus, when treated in a 1:1 mole ratio with propene sulfide, **38** is converted to the terminal, monosulfide cluster **46**, which is converted to the disulfide cluster **47** on further reaction with propene sulfide (Scheme 20). Cluster **47** is analogous to the dioxo cluster **43**, but it is indefinitely stable in air and unreactive towards further sulfur atom addition. In contrast, cluster **46** is slowly oxidized in air with loss of the sulfide ligand to give **43**. The $\mu_3$-S

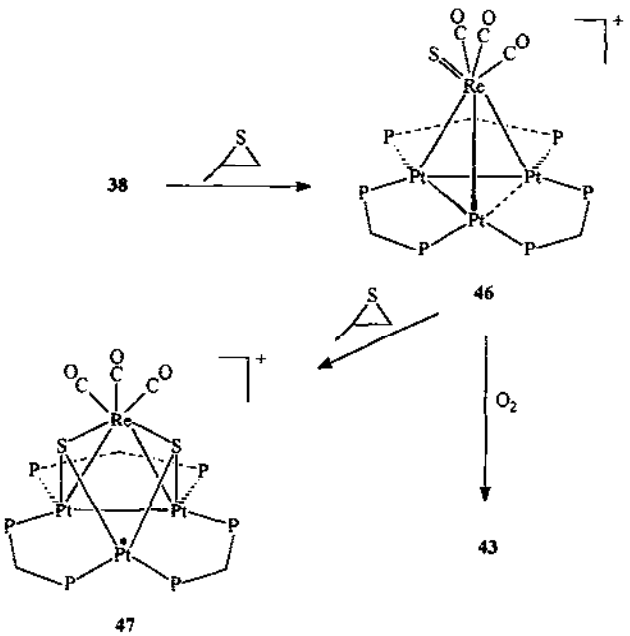


Scheme 20.

moiety is the most frequently observed coordination mode for sulfur in cluster complexes [119], but terminal Re=S groups are also known, for example in $[(S_4)_2ReS]^-$ [120].

The clusters **43** [107], **45** [110] and **47** [111] have been structurally characterized.

Table 8
Comparison of metal–metal distances in **38**, **43**, **45** and **47**[a]

| | **38**[b] | **43**[b] | **45**[c] | **47**[d] |
|---|---|---|---|---|
| Pt(1)–Pt(2) | 2.611(1) | 2.826(1) | 2.598(2) | 3.038(2) |
| Pt(1)–Pt(3) | 2.593(1) | 3.094(1) | 2.609(3) | 3.270(2) |
| Pt(2)–Pt(3) | 2.608(1) | 3.081(1) | 2.600(3) | 3.213(2) |
| Pt(1)–Re | 2.684(1) | 2.843(1) | 2.720(3) | 2.946(2) |
| Pt(2)–Re | 2.649(1) | 2.854(1) | 2.748(3) | 3.002(2) |
| Pt(3)–Re | 2.685(1) | 3.228(1) | 2.711(3) | 3.625(2) |

[a] In Å; see schemes for labelling. [b] Ref. [107]. [c] Ref. [110]. [d] Ref. [111].

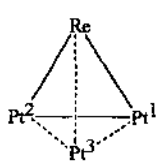

For comparison, the M–M bond distances of these clusters and **38** are given in Table 8. It is immediately clear that the incorporation of the $\mu_3$-O and $\mu_3$-S groups in **43** and **47** is accompanied by significant lengthening of all the M–M bonds, with respect to the M–M distances observed for **38**. In particular, the *Pt...M (M = Pt, Re) separations, where the *Pt centre is bound to both O or both S atoms, can be considered nonbonding. In contrast, the Pt–Pt bond distances in **45** are similar to those in **38** and, although the Pt–Re distances in **45** are somewhat greater than those in **38**, they still represent strong Pt–Re bonds. The overall transformation of **38** to **45** involves the replacement of the three carbonyl ligands in **38** by the three terminal oxo ligands in **45**. Since both CO and the terminal oxo ligand are formally two-electron donors, the overall cluster count in **38** and **45** are the same at 54-electrons. Hence, it is expected that the cluster cores should be similar. In contrast, clusters **43** and **47** are formed by the addition of two $\mu_3$-O and $\mu_3$-S ligands, which are four-electron donors, to **38** without carbonyl dissociation, and so are 62-electron clusters. Therefore, much weaker metal–metal bonding may be expected. The oxidation of **38** to **42**, **43** and **44**, involving sequential addition of 4-electron $\mu_3$-oxo ligands, leads to clusters with 58, 62 and 66-electron counts respectively, and so a progressive weakening of the M–M bonds is expected. No metal–metal bonding is expected for **44**. One consequence of the loss of metal–metal bonding, is a marked change in colours of the clusters. Thus, the intense red-black colour of **38**, which is associated with the metal–metal bonds, is replaced progressively by lighter colours and **44** is pale yellow in colour.

The trioxo cluster **45** reacts readily with donor ligands to give **48** or **49**. These reactions all occur at the $Pt_3$ centre according to Scheme 21 [121], in contrast to the reactions of **38** with neutral ligands, which occur at rhenium as shown in Scheme 17. These reactions with **45** (Scheme 21) are all reversible. Thus, for example, CO is readily lost from **49a** to regenerate **45**, and halide exchange reactions indicate that adduct formation is favoured in the order $I^- > Br^- > Cl^-$. The triply bridging carbonyl in **49a** is characterized in the IR by $\nu(CO) = 1606\ cm^{-1}$ and in the $^{13}C$ NMR by a 1:4:7:4:1 quintet at $\delta = 224.6$ with $^1J(PtC) = 513$ Hz. The terminal nature of the $P(OMe)_3$ ligand in the adduct **48** is shown by the low temperature $^{31}P$ NMR

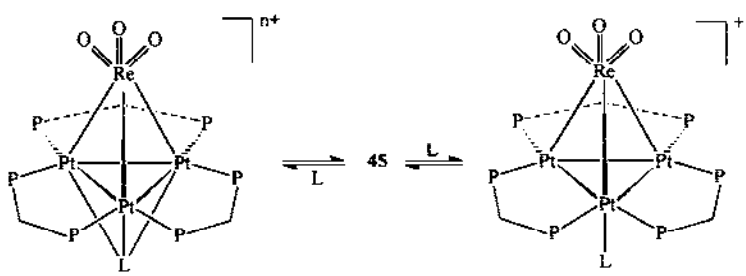


**49** (L = CO, n = 1, a; n = 0, L = $Cl^-$, b, $Br^-$, c; $I^-$, d)

**48** [L = $P(OMe)_3$]

Scheme 21.

spectrum, but the complex is fluxional due to easy migration of the phosphite ligand around the triangular $Pt_3$ face of the cluster.

The contrast between the selectivity towards ligand addition of **38** and **45** is dramatic, and shows how the site selectivity for ligand addition can be affected by the metal oxidation state [121]. It is interesting to note that, in the case of $Pt–Re/Al_2O_3$ catalysts, where both Re(0) and Re(IV) exist on the surfaces of the reduced catalyst, Re(0) is found to chemisorb CO, but Re(IV) shows no such activity [31]. The selectivity towards ligand addition of the clusters **38** and **45** can be considered to model this effect.

Scheme 22 outlines the reaction of the dioxo cluster **43** with donor ligands [114]. In contrast to the reactions of both **38** and **45**, the more electron-rich cluster complex **43** reacts by substitution of a carbonyl ligand at the rhenium centre. Thus, the reaction with $P(OR)_3$ gives a new dioxo species, **50**. This reaction resembles the reaction of $[\eta^5\text{-CpRe(CO)}_3]$ with neutral ligands under UV irradiation, where CO substitution instead of ligand addition usually takes place [115]. The reaction of **43** with $^{13}CO$ leads to carbonyl exchange and $^{13}C$ NMR monitoring showed that the reaction proceeds in a stepwise manner, eventually giving **51**.

The bonding in the 54-electron clusters **45** and **38** is similar, and so bonding in **45** can be understood in terms of the donation of electron density from the three filled Pt–Pt bonding orbitals of the $Pt_3(\mu\text{-dppm})_3$ fragment to the three vacant acceptor orbitals of the $Re(=O)^{3+}$ fragment [114]. In this formalism, the platinum and rhenium atoms in **45** may be considered as Pt(0) and Re(VII). Even though this is an extreme interpretation, the oxidation states of platinum and rhenium in **45** are clearly very different to an extent which is unprecedented in transition metal clusters. The difference in the oxidation state between Pt and Re in **43** is indeed seen in the core binding energies in these two atoms, as measured by the X-ray photoelectron spectra [114]. The binding energies in Pt and Re in **43** and related cluster complexes are presented in Table 9, together with $\nu$(CO) stretching frequencies for the corresponding clusters. The Re $4f_{7/2}$ binding energies in **38**, **42** to **44**, and **47** are essentially unchanged as more oxygen or sulfur atoms are added. In line with this observation, the values of $\nu$(CO) for the $Re(CO)_3$ groups also change only to a small extent in these clusters, so both parameters indicate little real change in the electron

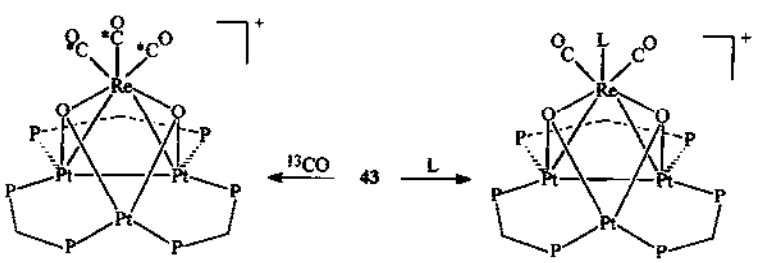


**51** (*C = $^{13}C$) **50** [L = $P(OMe)_3$, **a**, $P(OPh)_3$, **b**]

Scheme 22.

Table 9
Binding energies (eV)[a] and ν(CO) stretching frequencies of selected compounds

| Compound | Re $4f_{7/2}$ | Pt $4f_{7/2}$ | ν(CO) ($cm^{-1}$) |
|---|---|---|---|
| Pt (metal) | | 70.9[b] | |
| $PtCl_2$(dppm) | | 73.4[c] | |
| $[Pt_3(CO)(\mu\text{-dppm})_3]^{2+}$ | | 72.9 | 1765[c] |
| $[Pt_3\{Re(CO)_3\}(\mu\text{-dppm})_3]^+$, **38** | 41.6 | 72.6 | 1979, 1873, 1867[d] |
| $[Pt_3\{Re(CO)_3\}(\mu\text{-O})(\mu\text{-dppm})_3]^+$, **42** | 41.6 | 72.6 | 1978, 1864[d] |
| $[Pt_3\{Re(CO)_3\}(\mu\text{-O})_2(\mu\text{-dppm})_3]^+$, **43** | 41.6 | 73.0 | 1974, 1862, 1852[d] |
| $[Pt_3\{Re(CO)_3\}(\mu\text{-O})_3(\mu\text{-dppm})_3]^+$, **44** | 41.7 | 73.0 | 1987, 1856[d] |
| $[Pt_3(ReO_3)(\mu\text{-dppm})_3]^-$, **45** | 44.6 | 73.0[d] | |
| $[Pt_3\{Re(CO)_3S\}(\mu\text{-dppm})_3]^+$, **46** | 42.0 | 72.8 | 1979, 1874, 1850[e] |
| $[Pt_3\{Re(CO)_3\}(\mu\text{-S})_2(\mu\text{-dppm})_3]^+$, **47** | 41.7 | 73.0 | 1979, 1885, 1863[e] |

[a] Corrected with respect to C 1s BE of 284.9 eV. The anion is $PF_6^-$. [b] Ref. [27]. [c] Ref. [122]. [d] Ref. [114]. [e] Ref. [111].

density at rhenium. This result is interesting in that it shows that XPS binding energy does not always correlate with the oxygen content of the cluster. Therefore caution should be taken in correlating results obtained from XPS and TPR. The Pt $4f_{7/2}$ binding energy increases from 72.6 eV in **38** to 73.0 eV in **47** as the formal oxidation state of platinum increases from 0 to +II. The binding energies for the clusters overlap the ranges for Pt(I) and Pt(II) complexes [122]. In contrast, there is a large change in the Re $4f_{7/2}$ binding energy from 41.6 eV in **38** to 44.6 eV in the terminal oxo cluster **45** [114]. As can be seen from Table 2, the binding energy in $ReO_3$ is 44.9 eV. So it is very clear that rhenium is in a high oxidation state in **45**. Similarity, albeit less dramatically, formation of the Re=S group in **46** results in an increase in the Re $4f_{7/2}$ binding energy [111]. This is consistent with the result obtained for the silica-supported Pt–Re catalysts mentioned earlier [51].

## 5. Conclusions

### 5.1. Structure and bonding

A summary of the known structural data, based on X-ray structures, for known complexes containing Pt–Re bonds is given in Tables 7 and 8. A classification based on nuclearity and the number of cluster valence electrons (CVEs) is given in Table 10 and this table includes a number of compounds for which the structures were deduced from spectroscopic data only.

The Pt–Re distances in all the complexes discussed range from 2.65 to 3.00 Å. In these complexes, the average Pt–Re distances bridged by hydride (2.89 Å) and phosphide (av 2.85 Å) ligands are markedly longer, compared with the average Pt–Re distances having bridging carbonyl ligands (av 2.75 Å), and those without bridging ligands (av 2.77 Å). Therefore, on average, bridging hydride and phosphide ligands

Table 10
Electron counts and structures of Pt–Re clusters

| Entry | Cluster[a] | CVEs | Geometry | Ref. |
|---|---|---|---|---|
| 1 | $[PtReCp(CO)_2\{\mu\text{-}CR(OMe)\}L_2]$ | 32 | Binuclear | 66 |
| 2 | $[PtReCp(CO)_2(\mu\text{-}CR)L_2]^+$ | 32 | Binuclear | 66 |
| 4 | $[PtReCp(CO)_2(\mu\text{-}CS)L_2]$ | 32 | Binuclear | 68 |
| 6 | $[PtReCpH_2(CO)_2L_2]$ | 32 | Binuclear | 70a |
| – | $[PtReCp(\mu\text{-}CH_2)(CO)_2(PPh_3)_2]$ | 32 | Binuclear | 72b |
| 10 | $[PtReCpH(NO)(\mu\text{-}PR_2)L_2]^+$ | 32 | Binuclear | 74 |
| 11 | $[PtReCp(NO)(\mu\text{-}H)(\mu\text{-}PR_2)L_2]^+$ | 32 | Binuclear | 74 |
| 13 | $[PTRe(CO)_4(\mu\text{-}H)(\mu\text{-}CO)L_2]$ | 32 | Binuclear | 79 |
| 14 | $[PtRe(CO)Cl_2(N_2R)(\mu\text{-dppm})_2]$ | 32 | Binuclear | 82 |
| 23 | $[PtRe(CO)_5(\mu\text{-}CCR)L_2]$[b] | 32 | Binuclear[b] | 93 |
| 9 | $[PtReCpH(CO)(NO)(\mu\text{-}PR_2)L_2]^+$ | 34 | Pt Re abs. | 74 |
| 18 | $[PtRe_2(\mu\text{-}H)_2(CO)_8L_2]$ | 46 | Triangle | 85 |
| 19 | $[PtRe_2(\mu\text{-}H)_2(CO)_8(COD)]$ | 46 | Triangle | 87 |
| 20 | $[PtRe_2(\mu\text{-}CO)_2(CO)_8L]$ | 46 | Triangle | 91 |
| 21 | $[PtRe_2(\mu\text{-}H)(\mu\text{-}PR_2)(CO)_8L_2]$ | 46 | Triangle | 91 |
| 16 | $[PtRe_2(CO)_{12}]$ | 48 | Linear | 84 |
| 22 | $[PtRe_2(\mu\text{-}H)(\mu\text{-}CO)(\mu\text{-}PR_2)(CO)_8L]$ | 48 | Triangle? | 91 |
| 24 | $[PtRe_2(CO)_9(\mu\text{-}PR)(dppe)]$ | 48[c] | Angular | 94 |
| — | $[Pt_2Re(CO)_6(\mu\text{-dppm})_2]^+$ | 46 | Linear | 103 |
| 28 | $[PtRe_3(\mu\text{-}H)(CO)_{13}]^{2-}$ | 60 | Pseudoraft | 99 |
| 25 | $[PtRe_3(\mu\text{-}H)_3(CO)_{14}]$ | 62 | Spiked triangle | 87 |
| 33 | $[Pt_2Re_2(\mu\text{-}CO)_4(CO)_6L_2]$ | 58 | Butterfly | 88 |
| 36 | $[Pt_2Re_2(\mu\text{-}H)(\mu\text{-}CO)_2(CO)_6(\mu\text{-}PR_2)L_2]$ | 58 | Butterfly | 91 |
| 37 | $[Pt_2Re_2(\mu\text{-}CO)_2(CO)_6(\mu\text{-dppm})_2]$ | 58 | Diamond | 103 |
| — | $[Pt_2Re_2(\mu\text{-}CO)(CO)_8(\mu\text{-dppm})_2]$ | 60 | Spiked triangle | 103 |
| 38 | $[Pt_3Re(CO)_3(\mu\text{-dppm})_3]^+$ | 54 | Tetrahedral | 107 |
| 45 | $[Pt_3ReO_3(\mu\text{-dppm})_3]^+$ | 54 | Tetrahedral | 110 |
| 39 | $[Pt_3Re(CO)_3L(\mu\text{-dppm})_3]^+$ | 56 | Butterfly | 109 |
| 48 | $[Pt_3(ReO_3)L(\mu\text{-dppm})_3]^+$ | 56 | Tetrahedral | 121 |
| 42 | $[Pt_3Re(CO)_3(\mu_3\text{-}O)(\mu\text{-dppm})_3]^+$ | 58 | Butterfly? | 107 |
| 43 | $[Pt_3Re(CO)_3(\mu_3\text{-}O)_2(\mu\text{-dppm})_3]^+$ | 62 | [d] | 107 |
| 47 | $[Pt_3Re(CO)_3(\mu_3\text{-}S)_2(\mu\text{-dppm})_3]^+$ | 62 | [d] | 111 |
| 44 | $[Pt_3Re(CO)_3(\mu_3\text{-}O)_3(\mu\text{-dppm})_3]^-$ | 66 | [e] | 114 |
| 29 | $[PtRe_4(CO)_{17}]^{2-}$ | 74 | Pseudoraft | 99 |
| 26 | $[PtRe_4(\mu\text{-}H)_6(CO)_{16}]$ | 76 | Bow-tie | 86 |
| 27 | $[PtRe_4(\mu\text{-}H)_5(CO)_{16}]^-$ | 76 | Bow-tie | 86 |
| 34 | $[Pt_3Re_2(\mu\text{-}CO)_6(CO)_4L_3]$ | 70 | Trigonal bipyramidal[f] | 88 |
| 30 | $[PtRe_7C(CO)_{21}Me_3]^{2-}$ | 110 | bis-(capped) octahedron | 100 |

[a] L = $PR_3$. [b] R = $Re(CO)_4L$, there is no M–M bond for this Re atom. [c] Assuming PR is a 4e ligand. [d] $Pt_2Re$ triangle with third Pt atom having to M–M bonds. [e] No M–M bonds. [f] No PtPt bonding in trigonal plane.

tend to lengthen Pt–Re bonds, while bridging carbonyl ligands appear to shorten such bonds.

In most platinum and rhenium complexes the metals have 16-electron and 18-electron counts respectively and this feature is also observed in the compounds containing Pt–Re bonds. Thus the normal electron counting rules [1,2] need to be modified to allow for the presence of one or more 16-electron platinum centres in most of the compounds described in this review.

All of the known binuclear complexes containing Pt–Re single bonds have 32 CVEs (Tables 7 and 10), the required number to give 16- and 18-electron counts at Pt and Re respectively. The Pt–Re distances range from 2.731(1)–2.8815(8) Å with all but that for complex **23** in the narrow range 2.84–2.88 Å. Complex **9** has 34 CVEs and is presumed to have no PtRe bonding (Table 10).

The required electron count for a triangular $PtRe_2$ cluster is 46 CVEs and complexes **18**, **19** and **21** provide well-characterized examples. For these clusters, the Pt–Re distances are in the range 2.74–2.91 Å, with bonds bridged by hydride or $PR_2$ being longer than comparable unbridged bonds. The Re–Re distances are longer at 3.12–3.20 Å. There are three $PtRe_2$ clusters with 48 CVEs, namely the linear complex **16**, with two Pt–Re bonds and no Re–Re bond, the angular complex **24**, which has one Pt–Re and one Re–Re bond, and the cluster **22**, which is thought to be triangular. Theory predicts two M–M bonds and so both complexes **16** and **24** comply. The structure of cluster **22** has not been determined but, if the platinum retains the 16-electron configuration, theory would predict no Re–Re bond. The $Pt_2Re$ complex [OC Pt–Pt($\mu$-dppm)$_2$-Re(CO)$_5$] has 46 CVEs and since there are two 16-electron platinum centres, a structure with two M–M bonds is expected and this is consistent with the proposed linear structure.

In tetranuclear clusters, the preferred structure for a given electron count again depends on the number of platinum atoms. There appear to be no tetrahedral $PtRe_3$ clusters with six M–M bonds, for which 58 CVEs would be expected. The known $PtRe_3$ clusters are the 60-electron complex **28** and the 62-electron complex **25** and these have the diamond (or pseudo-raft) structure with five M–M bonds and the spiked triangle structure with four M–M bonds respectively, both being consistent with theory. Similarly, there are no tetrahedral $Pt_2Re_2$ clusters for which 56 CVEs would be expected, but all the structurally characterized clusters have the butterfly (complexes **33** and **36**) or diamond (complex **37**) structure with 58 CVEs and five M–M bonds. In the butterfly clusters, the missing bond is the PtPt bond whereas in the diamond structure it is the ReRe bond which is absent. The 60-electron cluster [$Pt_2Re_2$($\mu$-CO)(CO)$_8$($\mu$-dppm)$_2$] is proposed to have a spiked triangle structure with four M–M bonds (Scheme 16). The most highly coordinatively unsaturated clusters are the tetrahedral $Pt_3Re$ complexes **38** and **45** each of which has 54 CVEs. Addition of a ligand to the rhenium centre of **38** gives the 56-electron cluster **39** which has a butterfly structure (Scheme 17) and further ligand addition can occur to give 58- and 60-electron clusters with further loss of metal–metal bonding as indicated by spectroscopic studies (Scheme 18). However, addition of ligands to **45** occurs at the platinum centres and the 56-electron cluster products appear to retain the tetrahedral $Pt_3Re$ core; evidently one or more of the Pt centres adopts an 18-electron configura-

tion in the products **48** or **49** (Scheme 21) and the modified electron counting rules are no longer valid.

Perhaps the most impressive series of clusters is the set of formula $[Pt_3Re(CO)_3(\mu\text{-}O)_n(\mu\text{-}dppm)_3]^+$. The parent cluster is the 54-electron **38**, $n=0$, and since each $\mu_3$-O ligand contributes four electrons the product clusters have 58e when $n=1$, 62e when $n=2$ and 66e when $n=3$. Each O atom added should lead to loss of two M–M bonds so that, when $n=3$, there are no metal–metal bonds. Sulfur atom addition gives similar results but with greater increases in metal–metal distances as illustrated by the data in Table 8. Thus, the modified electron counting rules successfully account for the observed structures in this series.

There are no closed polyhedron pentanuclear PtRe clusters. The known $PtRe_4$ clusters include the 74-electron cluster **29** and the 76-electron clusters **26** and **27**, with raft (7 M–M bonds) and bow-tie (6 M–M bonds) structures respectively, consistent with theoretical predictions. The only other structurally characterized cluster is the unusual $Pt_3Re_2$ cluster **34** having 70 CVEs. This cluster has distorted trigonal bipyramidal geometry but with some very long M..M separations and so it is not clear how many M–M bonds are present. However, the structure is fully consistent with Mingos' rules [2], considering each Pt unit to cap the Re–Re bond so giving a cluster in which three $PtRe_2$ triangles are fused at the Re–Re edge.

The largest known clusters are the $PtRe_7$ clusters **30** and **31** each of which has 110 CVEs and, in both clusters, the platinum atoms have the 18-electron configuration.

In conclusion, most of the known PtRe clusters have the structures predicted from Wade's and Mingos' rules, modified to allow the platinum centres to have the 16-electron configuration. However, in some cases, one or more platinum atoms adopts the 18-electron configuration and so care must be taken in predicting structures based on these rules alone.

### 5.2. *Clusters and bimetallic catalysts*

There have been marked advances in our understanding of Pt–Re catalysis. In particular, the use of physical techniques such as EXAFS and studies of model reactions such as hydrogenolysis has provided much information on the structure and reactivity of the Pt–Re catalysts. However, there are still many questions that need to be answered.

It is interesting to compare the bond distances in the Pt–Re catalysts (Table 3) with those in structurally characterized PtRe clusters (Table 7). As mentioned, the known range of Pt–Re distances in clusters is 2.65–3.00 Å, with most falling in the range 2.7–2.9 Å, somewhat longer than the Pt–Re distance in Pt–Re catalysts. The range of Re–Re distances is 3.011–3.237 Å in clusters but only 2.73 Å in the Pt–Re catalyst. When Pt–Pt bonding is expected in the PtRe clusters, the range of Pt–Pt distances is 2.59–3.04 Å compared to 2.75 Å in the Pt–Re catalyst. There are also several clusters for which PtPt bonding is thought to be weak or absent but in which there are fairly short Pt..Pt contacts. For the complexes **33–36**, the range of such Pt..Pt distances is 2.982–3.159 Å and it overlaps with the range when Pt–Pt

bonding is expected. The shorter Pt–Re and Re–Re distances in the catalysts than in the clusters may reflect the greater degree of coordinative unsaturation in the PtRe alloy catalysts.

There are a number of cluster reactions which may be relevant to the function of Pt–Re catalysts. For example, in a number of cluster systems, the loss of CO ligand from a rhenium centre is greatly accelerated by a neighbouring platinum atom since the carbonyl may migrate from Re to Pt and then be easily displaced from the coordinatively unsaturated centre. Similar effects are observed with other unsaturated reagents (for example, Scheme 7) and such cooperative effects could obviously operate in the catalytic systems and aid the adsorption of reagents or the desorption of products from the catalyst surface.

The sulfidation of a $Pt_3Re$ cluster shown in Scheme 20 may well mimic the sulfidation of Pt–Re catalysts. For example, in both cases the initial sulfidation reaction occurs at rhenium and leads to lower reactivity at the rhenium centre. Similarly, the oxygen atom addition reactions shown in Scheme 19 may well mimic the reactions proposed to occur in the oxidation or reduction of Pt–Re catalysts. For example, the reactions may be the reverse of reactions leading to formation of Pt–Re alloy by catalytic reduction of perrhenate by platinum particles. The demonstration that compounds containing either ReOPt bridges or Pt–Re bonds can occur when rhenium is in a high oxidation state may provide a model for the binding of platinum to rhenium modified alumina surface. Given the formal oxidation states of Re can vary from fractional negative values in some anionic PtRe clusters to perhaps +6 or +7 in cluster **45**, covering most of the known range of oxidation states for rhenium [123], there appears to be scope for the discovery of many more unusual Pt–Re clusters which should add further insights into the remarkable properties of the heterogeneous Pt–Re catalysts.

## Acknowledgment

We thank the NSERC (Canada) for financial support.

## References

[1] D.F. Shriver, H.D. Kaesz and R.D. Adams (eds.), The Chemistry of Metal Cluster Complexes, VCH, New York, 1990.
[2] D.M.P. Mingos and D.J. Wales, Introduction to Cluster Chemistry, Prentice Hall, Englewood Cliffs, NJ, 1990.
[3] R.D. Adams and W.A. Herrmann, Polyhedron, 7 (1988) 2255–2463.
[4] L.J. Farrugia, Adv. Organomet. Chem., 31 (1990) 301.
[5] J.H. Sinfelt, Bimetallic Catalysts: Discoveries, Concepts and Applications, Wiley, New York, 1983.
[6] K.J. Klabunde and Y.-X. Li in M. E. Davis and S. L. Suib (eds.), Selectivity inCatalysis, ACS, Washington, DC, 1993.
[7] J. Biswas, G.M. Bickle, P.G. Gray, D.D. Do and J. Barbier, Catal. Rev. Sci. Eng., 30 (1988) 161.
[8] J.H. Sinfelt, Acc. Chem. Res., 20 (1987) 134.

[9] V. Ponec, Adv. Catal., 32 (1983) 149.
[10] D.A. King and D.P. Woodruff (eds.), The Chemical Physics of Solid Surfaces, Elsevier, New York, 6 (1993), Chapters 5 and 6.
[11] T.J. Henly, Coord. Chem. Rev., 93 (1989) 269.
[12] A. Perrin and M. Sergent, New. J. Chem., 12 (1988) 337.
[13] C.E. Holloway and M. Melnik, Organomet. Chem. Rev., 20 (1988) 249.
[14] B.C. Gates, Catalytic Chemistry, Wiley, New York, 1992.
[15] A.S. Fung, M.R. McDevitt, P.A. Tooley, M.J. Kelley, D.C. Koningsberger and B.C. Gates, J. Catal., 140 (1993) 190.
[16] J.L. Carter, G.B. Mcvicker, W. Weissman, W.S. Kmak and J.H. Sinfelt, Appl. Catal., 3 (1982) 327.
[17] H.E. Kluksdahl, US Patent, 3415, 737 (1968).
[18] L. Chen, Y. Ni, J. Zang, L. Lin, X. Luo and S. Chen, J. Catal., 145 (1994) 132.
[19] S.K. Purnell, J.-R. Chang and B.C. Gates, J. Phys. Chem., 97 (1993) 4196.
[20] J.H. Sinfelt and G.D. Meitzner, Acc. Chem. Res., 26 (1993) 1.
[21] A. Caballero, F. Villain, H. Dexpert, F. LePeltier and J. Lynch, J. Chem. Soc., Faraday Trans., 89 (1993) 159.
[22] F. Hilbrig, C. Michel and G.L. Haller, J. Phys. Chem., 96 (1992) 9893.
[23] D. Bazin, H. Dexpert, J.P. Bournonville and J. Lynch, J. Catal., 123 (1990) 86.
[24] C.M. Tsang, S.M. Augustine, J.B. Butt and W.M.H. Sachtler, Appl. Catal., 46 (1989) 45.
[25] S.M. Augustine and W.M.H. Sachtler, J. Catal., 116 (1989) 184.
[26] P. Malet, G. Munuera and A. Caballero, J. Catal., 115 (1989) 567.
[27] D.J. Godbey and G.A. Somorjai, Surf. Sci., 202 (1988) 204.
[28] W.T. Tysoe, F. Zaera and G.A. Somorjai, Surf. Sci., 200 (1988) 1.
[29] S.M. Augustine, M.S. Nacheff, C.M. Tsang, J.B. Butt and W.M.H. Sachtler, in M.J. Phillips and M. Ternan (eds.), Proceedings, 9th International Congress on Catalysis, Calgary, Canada, 3 (1988) 1190.
[30] G. Meitzner, G.H. Via, F.W. Lytle and J.H. Sinfelt, J. Phys. Chem., 87 (1987) 6354.
[31] M.S. Nacheff, L.S. Kraus, M. Ichikawa, B.M. Hoffman, J.B. Butt and W.M.H. Sachtler, J. Catal., 106 (1987) 263.
[32] S.M. Augustine and W.M.H. Sachtler, J. Catal., 106 (1987) 417.
[33] (a) J.H. Onuferko, D.R. Short and M.J. Kelley, Appl. Surf. Sci., 19 (1984) 227; (b) Z. Huang, J.R. Fryer, C. Park, D. Stirling and G. Webb, J. Catal., 148 (1994) 478.
[34] J.-R. Chang, L.U. Gron, A. Honji, K.M. Sanchez and B. C. Gates, J. Phys. Chem., 95 (1991) 9944.
[35] T. Beringhelli, G. Ciani, G. D'Alfonso, A. Sironi and M. Freni, J. Chem. Soc., Dalton Trans. (1985) 1507.
[36] P.S. Kirlin, F.B.M. van Zon, D.C. Koningsberger and B.C. Gates, J. Phys. Chem., 94 (1990) 8439.
[37] P. Spronk, J.A.R. van Veen and J.C. Mol, J. Catal., 144 (1993) 472.
[38] D.S. Kim and I.E. Wachs, J. Catal., 141 (1993) 419.
[39] R. Burch and A.J. Mithell, Appl. Catal., 6 (1983) 121.
[40] M.J. Kelley, R.L. Freed and D.G. Swartzfager, J. Catal., 78 (1982) 445.
[41] R.J. Bertolacini and R.J. Pellet, in B. Delmon and G.F. Forment (eds.), Catalyst Deactivation, Elsevier, New York, 1980.
[42] C. Bolivar, H. Charcosset, R. Fretty, M. Primet, L. Tournayan, C. Betizeau, G. Leclerq and R. Maurel, J. Catal., 39 (1975) 249.
[43] D.J. Godbey, F. Garin and G.A. Somorjai, J. Catal., 117 (1989) 144.
[44] G. Meitzner, G.H. Via, F.W. Lytle and J.H. Sinfelt, Phys. B, 158 (1989) 138.
[45] K.S. Liang, G.J. Hughes and J.H. Sinfelt, Phys. B, 158 (1989) 135.
[46] Y.U. Yermakov and B.N. Kuznetsov, J. Mol. Catal., 9 (1980) 13.
[47] K.I. Zamaraev and D.I. Kochubei, Kinet. Katal., 27 (1986) 891.
[48] R.W. Joyner, E.S. Shpiro, P. Johnston and G.J. Tuleuova, J. Catal., 141 (1993) 250.
[49] E.S. Shpiro, R.W. Joyner, P. Johnston and G.J. Tuleuova, J. Catal., 141 (1993) 266.
[50] V.K. Shum, J.B. Butt and W.M.H. Sachtler, J. Catal., 99 (1986) 126.
[51] P. Biloen, J.N. Helle, H. Verbeek, F.M. Dautzenberg and W.M.H. Sachtler, J. Catal., 63 (1980) 112.
[52] D.J. Godbey and G.A. Somorjai, Surf. Sci., 204 (1988) 301.

[53] S.M. Augustine and W.M.H. Sachtler, J. Phys. Chem., 91 (1987) 5953.
[54] A.J. den Hartog and V. Ponec, in M. Misono, Y. Moro-oka and S. Kimura (eds.), Future Opportunities in Catalytic and Separation Technology, Elsevier, New York, 1990, Chapter II. 5.
[55] J.A. Rodriguez and D.W. Goodman, Science, 257 (1992) 897.
[56] C.A. Querini and S.C. Fung, J. Catal., 141 (1993) 389.
[57] C.H. Bartholomew, P.K. Agrawal and J.R. Katzer, Adv. Catal., 31 (1982) 135.
[58] P.A. van Trimpont, G.B. Marin and G.F. Froment, Appl. Catal., 17 (1985) 161.
[59] Z. Schay, K. Matusek and L. Guczi, Appl. Catal., 10 (1984) 173.
[60] G.A. Somorjai, in L.L. Hegedus (ed.), Catalyst Design, Progress and Perspectives, Wiley, New York, 1987.
[61] S.M. Augustine, G.A. Alameddin and W.M.H. Sachtler, J. Catal., 115 (1989) 217.
[62] R.W. Coughlin, K. Kwakami and A. Hasan, J. Catal., 88 (1988) 150.
[63] J. Barbier, G. Corro, Y. Zhang, J.P. Bournville and J. P. Franck, Appl. Catal., 16 (1985) 169.
[64] R.D. Adams, in D.F. Shriver, H.D. Kaesz and R.D. Adams (eds.), The Chemistry of Metal Cluster Complexes, VCH, New York, 1990.
[65] F.G.A. Stone, Angew. Chem., Int. Ed. Engl., 23 (1984) 89.
[66] J.A.K. Howard, J.C. Jeffery, M. Laguna, R. Navarro and F.G.A. Stone, J. Chem. Soc., Dalton Trans., (1981) 751.
[67] J.C. Jeffery, R. Navarro, H. Razay and F.G.A. Stone, J. Chem. Soc., Dalton Trans., (1981) 2471.
[68] J.C. Jeffery, H. Razay and F.G.A. Stone, J. Chem. Soc., Dalton Trans., (1982) 1733.
[69] F.G.A. Stone, Acc. Chem. Res. 14 (1981) 318.
[70] (a) C.P. Casey, E.W. Rutter, Jr. and K.J. Haller, J. Am. Chem. Soc., 109 (1987) 6886; (b) C.P. Casey, Y. Wang, R.S. Tanke, P.N. Hazin and E.W. Rutter, Jr., New. J. Chem., 18 (1994) 43.
[71] C.P. Casey and E.W. Rutter, Jr., J. Am. Chem. Soc., 111 (1989) 8917.
[72] (a) C.P. Casey and Y. Wang, Organometallics, 11 (1992) 13; (b) C.P. Casey, Y. Wang, L.M. Petrovich, T.L. Underiner, P.N. Hazin and J.M. Desper, Inorg. Chim. Acta, 198–200 (1992) 557.
[73] J. Powell, M.R. Cregg and J.F. Sawyer, Inorg. Chem., 28 (1989) 4451.
[74] J. Powell, J.F. Sawyer and M.V.R. Stainer, Inorg. Chem., 28 (1989) 4461.
[75] J. Powell, J.C. Brewer, G. Gulia and J.F. Sawyer, Inorg. Chem., 28 (1989) 4470.
[76] W. Tam, G.-Y. Lin, W.-K. Wong, W.A. Kiel, V.K. Wong and A.J. Gladysz, J. Am. Chem. Soc., 104 (1982) 141.
[77] Q.-B. Bao, S.J. Geib, A.L. Rheingold and T.B. Brill, Inorg. Chem., 26 (1987) 3454.
[78] A. Pidcock, Adv. Chem. Ser., 196 (1982) 1.
[79] T. Beringhelli, G. d'Alfonso, A.P. Minoja and M. Freni, Gazz. Chim. Ital., 122 (1992) 375.
[80] O. Bars, P. Braunstein, G.L. Geoffroy and B. Metz, Organometallics, 5 (1992) 2021.
[81] S.J. Wang and R.J. Angellici, Inorg. Chem., 27 (1988) 3233.
[82] S.W. Carr, X.L.R. Fontaine, B.L. Shaw and M. Thornton-Pett, J. Chem. Soc., Dalton Trans., (1988) 769.
[83] B. Chaudret, B. Delavaux and R. Poilblanc, Coord. Chem. Rev., 86 (1988) 191.
[84] M.A. Urbancic, S.R. Wilson and J.R. Shapley, Inorg. Chem., 23 (1984) 2954.
[85] T. Beringhelli, A. Ceriotti, G. d'Alfonso and R.D. Pergola, Organometallics, 9 (1990) 1053.
[86] G. Ciani, M. Moret, A. Sironi, P. Antognazza, T. Beringhelli, G. d'Alfonso, R.D. Pergola and A. Minoja, J. Chem. Soc., Chem. Commun., (1991) 1255.
[87] P. Antognazza, T. Beringhelli, G. d'Alfonso, A. Minoja, G. Ciani, M. Moret and A. Sironi, Organometallics, 11 (1992) 1777.
[88] G. Ciani, M. Moret, A. Sironi, T. Beringhelli, G. d'Alfonso and R.D. Pergola, J. Chem. Soc., Chem. Commun., (1990) 1668.
[89] T. Beringhelli, G. d'Alfonso and A.P. Minoja, Organometallics, 10 (1991) 394.
[90] R.D. Wilson, S.M. Wu, R.A. Love and R. Bau, Inorg. Chem., 17 (1978) 1271.
[91] J. Powell, J.C. Brewer, G. Gulia and J.F. Sawyer, J. Chem. Soc., Dalton Trans., (1992) 2503.
[92] F.R. Hartley, in G. Wilkinson, F.G.A. Stone and E.W. Abel (eds.), Comprehensive Organometallic Chemistry, Pergamon, New York, 1982, Volume 6.
[93] T. Weidmann, V. Weinrich, B. Wagner, C. Robl and W. Beck, Chem. Ber., 124 (1991) 1363.
[94] S.I. Al-Resayes, P.B. Hitchcock and J.F. Nixon, J. Chem. Soc., Chem. Commun., (1987) 928.

[95] R.M. Bullock, L. Brammer, A.J. Schultz, A. Albinati and T.F. Koetzle, J. Am. Chem. Soc., 114 (1992) 5125.
[96] C.S. Yang, C.P. Cheng, L.W. Guo and Y.J. Wang, Chin. Chem. Soc. (Taipei), 32 (1985) 17.
[97] T. Beringhelli, G. Ciani, G. d'Alfonso, L. Garlaschelli, M. Moret and A. Sironi, J. Chem. Soc., Dalton Trans., (1992) 1865.
[98] T. Beringhelli, G. d'Alfonso and A.P. Minoja, Organometallics, 13 (1994) 663.
[99] T. Beringhelli, A. Ceriotti, G. Ciani, G. d'Alfonso, L. Garlaschelli, R.D. Pergola, M. Moret and A. Sironi, J. Chem. Soc., Dalton Trans. (1993) 199.
[100] T.J. Henly, J.R. Shapley, A.L. Rheingold and S.J. Geib, Organometallics, 7 (1988) 441.
[101] C.-M.T. Hayward and J.R. Shapley, Organometallics, 7 (1988) 448.
[102] M.R. Churchill, B.G. DeBoer and F.J. Rotella, Inorg. Chem., 15 (1976) 1843.
[103] J. Xiao, J.J. Vittal and R.J. Puddephatt, J. Chem. Soc., Chem. Commun., (1993) 167.
[104] P. Braunstein, C. de Meric de Bellefon, S.E. Bouaoud, D. Grandjean, J.F. Halet and J.Y. Saillard, J. Am. Chem. Soc., 113 (1991) 5282.
[105] P. Braunstein, C. de Meric de Bellefon, M. Ries, J. Fischer and S.E. Bouaoud, Inorg. Chem., 27 (1988) 1327.
[106] R.J. Puddephatt, Lj. Manojlović-Muir and K.W. Muir, Polyhedron, 9 (1990) 2767.
[107] J. Xiao, J.J. Vittal, R.J. Puddephatt, Lj. Manojlović-Muir and K.W. Muir, J. Am. Chem. Soc., 115 (1993) 7882.
[108] J. Xiao, J.J. Vittal and R.J. Puddephatt, J. Organomet. Chem., in press.
[109] J. Xiao, R. J. Puddephatt, Lj. Manojlović-Muir and K.W. Muir, Organometallics, in press.
[110] J. Xiao, R.J. Puddephatt, Lj. Manojlović-Muir and K.W. Muir, J. Am. Chem. Soc., 116 (1994) 1129.
[111] L. Hao, J. Xiao, J.J. Vittal and R.J. Puddephatt, J. Chem. Soc., Chem. Commun., (1994) 2183.
[112] (a) C.P. Casey and J.M. O'Connor, Chem. Rev., 87 (1987) 307;
(b) C.P. Casey, R.A. Widenhoefer and J.M. O'Connor, J. Organomet. Chem., 428 (1992) 99.
[113] J. Xiao, R.J. Puddephatt, Lj. Manojlović-Muir and K.W. Muir, unpublished work, 1994.
[114] M.-G. Choi and R.J. Angelici, J. Am. Chem. Soc., 113 (1991) 5651.
[115] W.A. Herrmann, Angew. Chem., Int. Ed. Engl., 27 (1988) 1297.
[116] W.A. Nugent and J.M. Mayer, Metal-Ligand Multiple Bonds, Wiley, New York, 1988.
[117] F. Bottomley and L. Sutin, Adv. Organomet. Chem., 28 (1988) 339.
[118] C.E. Housecroft, in T.P. Fehlner (ed.), Inorganometallic Chemistry, Plenum Press, New York, 1992.
[119] A. Müller, E. Krickemeyer, H. Bogge, M. Penk and D. Rehder, Chimia, 40 (1986) 50.
[120] J. Xiao, L. Hao, R.J. Puddephatt, Lj. Manojlović-Muir and K.W. Muir, J. Chem. Soc., Chem. Commun., (1994) 2221.
[121] M.C. Jennings, G. Schoettel and R.J. Puddephatt, Organometallics, 10 (1991) 580.
[122] F. A. Cotton and G. Wilkinson, Advanced Inorganic Chemistry, Wiley, New York, 1988.